TITLE

Immune checkpoint proteins are conserved across 160 million years of evolution and are expressed on transmissible cancers

RUNNING TITLE

Transmissible cancers express evolutionarily conserved immune checkpoint molecules

AUTHORS

Andrew S. Flies[1]*, Jocelyn M. Darby[1], Patrick R. Lennard[1,2], Peter R. Murphy[1,3], Chrissie E. B. Ong[1], Terry L. Pinfold[4], A. Bruce Lyons[4], Gregory M. Woods[1], Amanda L. Patchett[1]

AFFILIATIONS

[1]Menzies Institute for Medical Research, College of Health and Medicine, University of Tasmania, Hobart, TAS 7000, Australia

[2]The Roslin Institute and Royal School of Veterinary Studies, University of Edinburgh, Easter Bush Campus, Midlothian, EH25 9RG, UK

[3]University of Queensland Diamantina Institute, The University of Queensland, Translational Research Institute, Woolloongabba, Queensland, Australia

[4]School of Medicine, College of Health and Medicine, University of Tasmania, Hobart, TAS 7000, Australia

CORRESPONDING AUTHOR CONTACT INFORMATION

Andrew S. Flies, PhD

Menzies Institute for Medical Research, College of Health and Medicine

University of Tasmania

Private Bag 23, Hobart TAS 7000

phone: +61 3 6226 4614; email: Andy.Flies@utas.edu.au

GRAPHICAL ABSTRACT

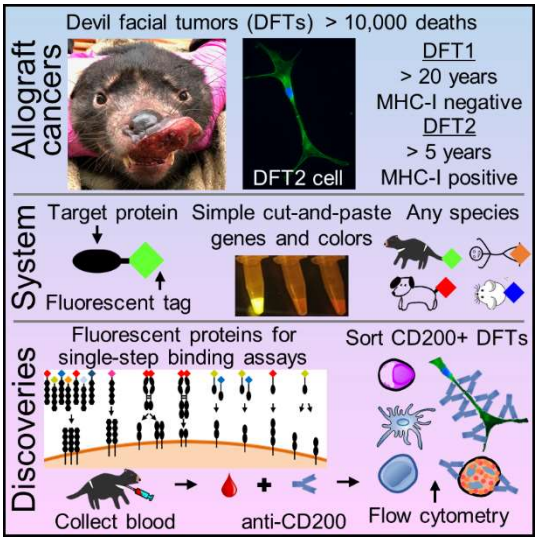

SIGNIFICANCE

Immune checkpoint immunotherapy has revolutionized medicine, but translational success for new treatments remains low. Around 40% of humans and Tasmanian devils (*Sarcophilus harrisii*) develop cancer in their lifetime, compared to less than 10% for most species. Additionally, devils are affected by two of the three known transmissible cancers in mammals. Unfortunately, little is known about the role of immune checkpoints in devils and other non-model species, largely due to a lack of species-specific reagents. We developed a simple cut-and-paste reagent development method applicable to any vertebrate species and show that immune checkpoint interactions are conserved across 160 million years of evolution. The inhibitory checkpoint molecule CD200 is highly expressed on devil facial tumor cells. We are the first to demonstrate that co-expression of CD200R1 can block CD200 expression. The evolutionarily conserved pathways suggest that naturally occurring cancers in devils and other species can serve as models for understanding cancer and immunological tolerance.

41 **ABSTRACT**

42 Around 40% of humans and captive Tasmanian devils (*Sarcophilus harrisii*) develop cancer,
43 compared to less than 10% for most species. Tasmanian devils also suffer from two of the three
44 known naturally-occurring transmissible cancers detected in vertebrate species. Transmissible
45 cancers are a unique form of cancer in which tumor cells act as an infectious pathogen and an
46 allograft. The two different transmissible devil facial tumors (DFT1 and DFT2) overcome
47 immunological barriers (e.g. major histocompatibility complex) and have killed thousands of
48 devils. Immune checkpoint immunotherapy has revolutionized human oncology in recent years.
49 However, immune checkpoints in transmissible and non-transmissible cancers remains largely
50 unexplored in most species due to a lack of species-specific reagents. To overcome this, we
51 developed a "cut-and-paste" Fluorescent Adaptable Simple Theranostic (FAST) protein system,
52 adaptable for any vertebrate species. This method facilitated rapid confirmation of seven receptor-
53 ligand interactions between twelve immune checkpoint proteins in Tasmanian devils, thus filling
54 a 160 million year gap in our understanding of the evolution of the mammalian immune system.
55 We used this system to investigate the checkpoint molecule CD200, which can inhibit natural killer
56 cell responses to cancer and facilitate graft tolerance in humans and mice. CD200 was highly
57 expressed on DFT cells and can be used to identify DFT cells in devil blood. Understanding how
58 transmissible tumor cells graft onto new hosts and evade immune defenses will help to identify
59 evolutionarily conserved immunological principles relevant to transplant immunology, cancer, and
60 infectious disease for human and veterinary medicine.

61 **KEYWORDS**

62 immune checkpoint, wild immunology, reagent development, marsupial, transmissible cancer

63 **INTRODUCTION**

64 Metastatic cancer affects most mammals, but the cancer incidence can vary widely across
65 phylogenetic groups and species (**Figure 1, Table S1**) [1–9]. In humans, the lifetime risk of
66 developing cancer is around 40% [10]. This is in stark contrast to a general cancer incidence of 3%
67 for mammals, 2% for birds, and 2% for reptiles reported by the San Diego Zoo (n=10,317) [7,11]. A
68 more recent study at the Taipei Zoo reported cancer incidence of 8%, 4%, and 1% for mammals,
69 birds, and reptiles, respectively (n=2,657) [4]. Cancer incidence in domestic animals is generally less
70 than 10% (n=202,277) [9]. However, two studies performed 40 years apart reported that greater than
71 40% of Tasmanian devils develop spontaneous, often severe neoplasia in their lifetime [11,12]. Devils
72 are also unique because they are affected by two of the three known naturally-occurring
73 transmissible cancers in vertebrate species [13,14]. Transmissible cancers are a distinct form of cancer
74 in which the tumor cells function as an infectious pathogen and an allograft. Dogs (*Canis lupus*
75 *familiaris*) are the only other vertebrate species affected by a transmissible cancer [15], and
76 interestingly some breeds of dogs also have high cancer incidence [9,16].

77 The devil facial tumor (DFT) disease was first detected in Northwest Tasmania and has
78 been a primary driver of an 80% decline in the wild Tasmanian devil population [13,17]. The clonal
79 devil facial tumor (DFT1) cells have been continually transmitted among devils and is estimated
80 to have killed at least 10,000 individuals since at least 1996. In 2014 a second independent
81 transmissible Tasmanian devil facial tumor (DFT2) was discovered in wild devils [14] and 23 cases
82 have been reported to date [18]. Genetic mismatches, particularly in the major histocompatibility
83 complex (MHC) genes should lead to rejection of these transmissible tumors. Consequently, the
84 role of devil MHC has been a focus of numerous studies (**Figure 1, Table S1**) to understand the
85 lack of rejection of the transmissible tumors. These studies have revealed that the DFT1 cells

86 downregulate MHC class I (MHC-I) expression [19], a phenomenon observed in many human
87 cancers [20]. In contrast to DFT1 cells, the DFT2 cells do express MHC-I [21]. DFT1 and DFT2 cells
88 also have 2,884 and 3,591 single nucleotide variants, respectively, that are not present in 46 normal
89 devil genomes [22]. The continual transmission of DFT1 and DFT2, despite MHC-I expression by
90 DFT2 cells and genetic mismatches between host and tumor, suggests that additional pathways are
91 likely involved in immune evasion.

92 Human cancer treatment has been revolutionized in the past decade by manipulating
93 interactions among immune checkpoint molecules [23,24]. These have proven broadly effective in
94 part because they function across many different MHC types and tumor mutational patterns.
95 However, these pathways have received little attention in transmissible cancers and other naturally
96 occurring cancers in non-model species (**Figure 1, Table S1**) [25–27]. We have previously shown that
97 the inhibitory immune checkpoint molecule programmed death ligand 1 (PDL1) is expressed in
98 the DFT microenvironment and is upregulated by interferon-gamma (IFNγ) *in vitro* [25]. This finding
99 led us to question which other immune checkpoint molecules play a role in immune evasion by
100 the transmissible cancers and the devil's high spontaneous cancer incidence. Understanding this
101 immune evasion in a natural environment has the potential to help protect this endangered species
102 and identify protein interactions that are conserved across divergent species to improve
103 translational success of animal models [27]. Unfortunately, a persistent limitation for immunology
104 in non-traditional study species is a lack of species-specific reagents. Wildlife biologists and
105 veterinarians are at the front lines of emerging infectious disease outbreaks, but they often lack
106 species-specific reagents to fulfil the World Health Organization's call for "cross-cutting R&D
107 preparedness" and perform mechanistic immunological investigations [28].

108 To solve the paucity of reagents available for Tasmanian devils and address ongoing
109 limitations for non-traditional study species, we developed a Fluorescent Adaptable Simple
110 Theranostic (FAST) protein system that builds upon the diverse uses of fluorescent proteins
111 previously reported [29–33]. This simple system can be used for rapid development of diagnostic and
112 therapeutic (i.e. theranostic) immunological toolkits for any animal species (**Figure 2**). We
113 demonstrate the versatility and impact of the FAST system by using it to confirm seven receptor-
114 ligand interactions among twelve checkpoint proteins in devils.

115 In humans, these checkpoint proteins have been targets of immunotherapy in clinical trials,
116 but the functional role and binding patterns of these proteins are unknown for most other species.
117 We have used the FAST system to show that the inhibitory checkpoint protein CD200 is highly
118 expressed on DFT cells, opening the door to single-cell phenotyping of circulating tumor cells
119 (CTCs) in devil blood. Furthermore, we are the first to report that co-expression of CD200R1 can
120 block surface expression of CD200 in any species. Understanding how clonal tumor cells graft
121 onto new hosts, evade immune defenses and metastasize within a host will identify evolutionarily
122 conserved immunological mechanisms to help improve cancer, infectious disease, and transplant
123 outcomes for human and veterinary medicine.

124

125 **RESULTS**

126 **Fluorescent fusion proteins can be secreted from mammalian cells**

127 Initially, we developed FAST proteins to determine whether monomeric fluorescent
128 proteins could be fused to devil proteins and secreted from mammalian cells (**Figure 2A** and **Table**
129 **S2**). We used 41BB (TNFRSF9) for proof-of-concept studies by fusing the extracellular domain
130 of devil 41BB checkpoint molecule to monomeric fluorescent proteins (**Figure 2A-B** and **Figure**

131 **S1**). We used wild-type Chinese hamster ovary (CHO) cells and CHO cells transfected with
132 41BBL (TNFSF9) to confirm specificity of the 41BB FAST proteins and demonstrate that the
133 fluorescent proteins (mAzurite, mCerulean3, mCherry, mCitrine, mOrange, Neptune2, and mTag-
134 BFP (aka mBFP)) remained fluorescent when secreted from mammalian cells (**Figure 2C**).

135 We chose mCherry, mCitrine, mOrange, and mBFP for ongoing FAST protein
136 development. Initial batches of FAST proteins were purified using the 6xHis-tag and eluted with
137 imidazole. The gradient of FAST protein in the collection tubes was apparent when excited with
138 blue light and visualized with an amber filter unit (**Figure 2D**), allowing immediate confirmation
139 that the fluorescent protein DNA coding sequences were in-frame and the proteins were properly
140 folded. mCherry was visible without excitation or filters (**Figure 2E**). After combining,
141 concentrating, and sterile filtering the eluted fractions, 100 µL was aliquoted and visualized again
142 using blue light to confirm fluorescent signal (**Figure 2F**). A full step-by-step protocol and set of
143 experimental templates for creating and testing FAST proteins for any species is available online
144 with the supplementary material.

145 **Receptor-ligand binding confirmed in single-step staining assays**

146 We chose additional immune checkpoint molecules for FAST protein development
147 (**Figure 3A**) based on targets of clinical trials and sequence analysis of devil genes [27,34,35]. We
148 transfected the FAST protein expression vectors (**Table S2**) into CHO cells and tested the
149 supernatant against CHO cell lines expressing full-length receptors. 41BB FAST proteins in
150 supernatant exhibited strong binding to 41BBL cell lines, but the fluorescent signals from most
151 other FAST proteins were too weak to confirm binding to the expected receptors (**Figure S2**). As
152 FAST proteins do not require secondary reagents, we next incubated target cells with purified
153 FAST proteins and added chloroquine to block the lysosomal protein degradation pathway [36]. This

154 allowed us to take advantage of receptor-mediated endocytosis, which can allow accumulation of
155 captured fluorescent signals inside the target cells [37]. This protocol adjustment allowed
156 confirmation that CD47-mCherry, CD200-mBFP, CD200-mOrange, CD200R1-mBFP, and
157 CD200R1-mOrange, and PD1-mCitrine bound to their expected receptors (**Figure 3B**). We also
158 demonstrated the flexibility of the FAST proteins by showing that alternative fusion conformations
159 (**Figure S1C-D**), such as type II proteins (e.g. mCherry-41BBL) and a devil Fc-tag (e.g. CD80-
160 Fc-mCherry) bound to their expected ligands (**Figure 3B**). The stability of the fusion proteins was
161 demonstrated using supernatants that were stored at 4 °C for two months prior to use in a one-hour
162 live-culture assay with chloroquine (**Figure S3**).

163 **Cell lines secreting FAST proteins confirm protein interactions in live coculture assays**

164 To further streamline the reagent development process, we next took advantage of the
165 single-step nature of FAST proteins (i.e. no secondary antibodies or labels needed) in live-cell
166 coculture assays (**Figure 4A**). Cell lines secreting 41BB-mCherry, 41BBL-mCherry, or CD80-Fc-
167 mCherry FAST proteins were mixed with cell lines expressing full-length 41BB, 41BBL, or
168 CTLA4-mCitrine and cocultured at a 1:1 ratio overnight with chloroquine. Singlet cells were gated
169 (**Figure 4B**) and binding of mCherry FAST proteins to CFSE or mCitrine-labelled target cells was
170 analyzed (**Figure 4C**). The strongest fluorescent signal from 41BB-mCherry, 41BBL-mCherry
171 and CD80-Fc-mCherry were detected when cocultured with their predicted receptors, 41BBL,
172 41BB and CTLA4, respectively.

173 **Optimization of the FAST-Fc construct**

174 The fluorescent binding signal of CD80-Fc-mCherry was lower than expected, so we next
175 re-examined our Fc-tag construct. In humans and all other mammals examined to date the IgG
176 heavy chain has glycine-lysine (Gly-Lys) residues at the C-terminus [38]; the initial devil IgG

177 constant region sequence available to us had an incomplete C-terminus, and thus our initial CD80-
178 Fc-mCherry vector did not have the C-terminal Gly-Lys. We subsequently made a new FAST-Fc
179 construct with CTLA4-Fc-mCherry, which exhibited strong binding to both CD80 and CD86
180 transfected DFT cells (**Figure 4D**).

181 **CD200 mRNA and protein are highly expressed in DFT cells**

182 Analysis of previously published devil and DFT cell transcriptomes suggested that CD200
183 mRNA is highly expressed in DFT2 cells and peripheral nerves, moderately expressed in DFT1
184 cells, and lower in other healthy devil tissues (**Figure 5A**) [34,35,39]. As CD200 is an inhibitory
185 molecule expressed on most human neuroendocrine neoplasms [40], and both DFT1 and DFT2
186 originated from Schwann cells [35,41], we sought to investigate CD200 expression on DFT cells at
187 the protein level. Staining of wild-type DFT1 and DFT2 cells with CD200R1-mOrange FAST
188 protein showed minimal fluorescent signal (**Figure 5B**). However, overexpression of CD200 using
189 a human EF1α promoter yielded a detectable signal with CD200R1-mOrange binding to CD200
190 on DFT1 cells. A weak signal from CD200-mOrange was detected on DFT1 cells overexpressing
191 CD200R1 (**Figure 5B**). To confirm naturally-expressed CD200 on DFT cells we digested CD200
192 and 41BB FAST proteins using TEV protease to remove the linker and fluorescent reporter. The
193 digested proteins were then used to immunize mice for polyclonal sera production. We stained
194 target CHO cell lines with pre-immune (PI) or immune (I) mouse sera collected after 3X
195 immunizations. Only the immune sera showed strong binding to the respective CD200 and 41BB
196 target cell lines (**Figure 5C**). After the final immunization (4X), we collected another batch of sera
197 and tested it on DFT1 and DFT2 cells (**Figure 5D**). In agreement with the transcriptomic data for
198 DFT cells [34], the polyclonal sera revealed high levels of CD200 on DFT cells, but low levels of
199 41BB.

200 **Overexpression of CD200R1 blocks surface expression of CD200**

201 In humans, overexpression of some checkpoint proteins can block surface expression of
202 heterophilic binding partners in *cis* (e.g. CD80 and PDL1) [42,43]. As a potential route for disrupting
203 the inhibitory effects of CD200 on anti-tumor immunity, we tested if overexpression of CD200R1
204 on DFT cells could reduce CD200 surface expression. We stained a DFT1 strain C5065, and DFT1
205 C5065 cells transfected to overexpress CD200 or CD200R1 with polyclonal anti-CD200 sera and
206 secondary anti-mouse IgG AF647. We detected no surface protein expression of CD200 DFT1
207 cells overexpressing CD200R1 (**Figure 5E**).

208 **Identification of DFT cells in whole blood using anti-CD200**

209 In addition to high expression of CD200 on neuroendocrine neoplasms [40,44], CD200 is used
210 as a diagnostic marker for several human blood cancers [45–47]. DFT cells metastasize in the majority
211 of cases [48] and our transcriptome results (**Figure 5A**) suggest that CD200 mRNA is more highly
212 expressed in DFT cells than in peripheral blood mononuclear cells (PBMCs) [34,35]. As a result, we
213 tested if CD200 could be used to identify DFT cells in blood. We stained PBMCs and DFT2 cells
214 separately with polyclonal anti-CD200 sera and anti-mouse AlexaFluor 647 and then analyzed
215 CD200 expression by flow cytometry (**Figure S4A**). We then mixed the stained PBMCs and DFT2
216 cells at ratios of 1:10 (**Figure S4A**) and 1:5 (**Figure S4B**) and analyzed the mixed populations.
217 PBMCs showed minimal CD200 expression and background staining (**Figure S4**), whereas
218 CD200 was highly expressed on DFT2 cells. CD200+ DFT2 cells were readily distinguishable
219 from PBMCs.

220 As our RNAseq results only included mononuclear cells, we next performed a pilot test to
221 determine if DFT cells could be spiked into whole devil blood and identified via flow cytometry
222 using CD200 staining. DFT1 and DFT2 cells were labeled with CellTrace violet (CTV) and 10,000

223 cells were diluted directly into 100 μL of whole blood from a healthy devil (n=1/treatment; n = 1
224 devil). The cells were then stained with purified polyclonal anti-CD200 with and without
225 secondary anti-mouse IgG AF647 prior to red blood cell (RBC) lysis. Initial results showed that
226 DFT2 cells expressed CD200 above the leukocyte background, but that DFT1 cells could not be
227 distinguished from leukocytes (**Figure S5**). To eliminate the secondary antibody step from the
228 whole blood staining protocol we next labelled the polyclonal anti-CD200 and normal mouse
229 serum (NMS) with a no-wash Zenon mouse IgG AF647 labeling reagent (n = 1/treatment; n = 2
230 devils). This system again showed that CD200 expression could be used to identify DFT2 cells in
231 blood (**Figure 6**), suggesting that CD200 is a candidate marker for identification of metastasizing
232 DFT2 cells.
233

234 **DISCUSSION**

235 Naturally occurring cancers provide a unique opportunity to study immune evasion and the
236 metastatic process across diverse hosts and environments. The exceptionally high cancer rate in
237 Tasmanian devils coupled with the two transmissible tumors currently circulating in the wild
238 warrants a thorough investigation of the devil immune system. However, taking advantage of such
239 natural disease models has been out of reach for most species due to a lack of reagents. The FAST
240 protein system we developed here is well-suited to discovering additional DFT markers, and more
241 generally, filling the reagent gap for non-traditional species. For proteins like 41BB that have high
242 affinity for 41BBL, FAST proteins can be used as detection reagents directly from supernatant.
243 For other molecules with lower receptor-ligand affinity, the FAST proteins can be purified,
244 digested with a protease to remove the non-target proteins and used for production of polyclonal
245 or monoclonal antibodies.

246 The simple cut-and-paste methods for vector assembly lend the FAST protein system to
247 entry level immunology and molecular biology skill sets. Additionally, the ability of FAST
248 proteins to be used in live coculture assays and with elimination of secondary reagents, will
249 increase efficiency and reduce experimental error for advanced human and mouse cancer
250 immunology studies. For example, previous high-throughput studies have used a two-step staining
251 process (i.e. recombinant protein + secondary antibody) to screen more than 2000 protein
252 interactions [49,50]; this type of assay can be streamlined using FAST proteins to eliminate the need
253 for secondary antibodies. Fc-tags or other homodimerization domains can be incorporated into
254 FAST proteins to increase binding for low-affinity interactions.

255 Production of recombinant proteins in cell lines that closely resemble the physiological
256 conditions of the native cell type (i.e. mammalian proteins produced in mammalian cell lines) are
257 more likely to yield correct protein folding, glycosylation, and function than proteins produced
258 using evolutionarily distant cell lines [51]. The fluorescent fusion proteins developed here that take
259 advantage of natural receptor expression and cycling processes (e.g. CTLA4 transendocytosis) in
260 eukaryotic target cells; bacterial protein production methods are not amenable to coculture with
261 eukaryotic target cells in immunological assays [52]. Our demonstration of the FAST protein system
262 in CHO cells, which are used to produce approximately 70% of recombinant pharmaceutical
263 proteins [53], suggest that this method can be efficiently integrated into existing research and
264 development pipelines for humans and other vertebrate species.

265 A primary question in transmissible tumor research is why genetically mismatched cells
266 are not rejected by the host. Successful infection of devils with DFT cells relies on the ability of
267 the tumor allograft to evade and manipulate host defences. The "missing-self" hypothesis suggests
268 that the lack of constitutive MHC-I expression on DFT1 cells should lead to natural killer (NK)

269 cell-mediated killing of the allograft tumor cells. Here we used the FAST protein system to develop
270 a tool set to address this question and show that DFT1 and DFT2 cells express CD200 at higher
271 levels than most other devil tissues examined to date. CD200 has been shown to directly inhibit
272 NK cells in other species [54–56], so overexpression of CD200 is a potential mechanism of immune
273 evasion of NK responses by DFT cells.

274 We hypothesize that CD200 could be particularly important in DFT transmission as the
275 CD200-CD200R pathway is critical to the initial stages of establishing transplant and allograft
276 tolerance in other species [57–59]. In line with this hypothesis, a recent study reported that
277 overexpressing several checkpoint molecules, including CD200, PDL1, and CD47, in mouse
278 embryonic stem cells could be used to generate teratomas that could establish long-term allograft
279 tolerance in fully immunocompetent hosts [60]. We have previously reported that PDL1 mRNA and
280 protein are upregulated on DFT2 cells in response to IFNγ [25], and our transcriptome results show
281 that CD47 is expressed at moderate to high levels in DFT cells. Here we show that overexpression
282 of CD200R1 on DFT1 eliminates binding of our polyclonal anti-CD200 antibodies, suggesting
283 that DFT cells overexpressing CD200R1 could be used to test the role of CD200 in allograft
284 tolerance. Alternatively, genetic ablation of CD200 in DFT cells could be used as a complementary
285 approach to examine the role of immune checkpoint molecules in DFT allograft tolerance. The
286 CD200-CD200R1 pathway has been implicated in reducing IFNγ production by dendritic cells [59]
287 and decreasing the responsiveness of myeloid cells to IFNγ stimulation [61]. Low MHC-I expression
288 is a primary means of immune evasion by DFT1 cells, and disrupting the CD200-CD200R1
289 pathway could facilitate improved recognition of DFT1 cells by CD8 T cells by enhancing IFNγ-
290 mediated MHC-I upregulation. Recent work in mice has identified immunosuppressive natural

291 regulatory plasma cells that express CD200, LAG3, PDL1, and PDL2; we have previously
292 identified PDL1+ cells with plasma cell morphology near or within the DFT microenvironment [25].
293 Previous DFT vaccine efforts have used killed DFT cells with adjuvants [62,63]. A similar
294 approach to treat gliomas in dogs reported that tumor-lysate with CD200 peptides nearly doubled
295 progression-free survival compared to tumor lysate alone [64]. Like devils, several breeds of dog are
296 prone to cancer and these genetically-outbred large animal models provide a fertile ground for
297 testing cancer therapies. Interestingly, the CD200 peptides are reported to provide agonistic
298 function through CD200-like activation receptors (CD200R4) rather than by blocking CD200R1
299 [44,64]. The functional role of CD200-CD200R pathway in devils remains to be elucidated, but the
300 $CD200R1_{NPLY}$ inhibitory motif and key tyrosine residues are conserved in devil CD200R [27,65,66],
301 demonstrating this motif is conserved over 160 million years of evolutionary history [67]. In addition
302 to agonistic peptides, several other options for countering CD200-CD200R immune inhibition are
303 possible. Human chronic lymphocytic leukemia cells often express high levels of CD200, which
304 can be downregulated in response to imiquimod [68]. Likewise, we have previously shown that DFT1
305 cells downregulate expression of CD200 mRNA *in vitro* in response to imiquimod treatment [34].
306 In mice, chronic salmonella and schistosoma infections upregulated both CD200 and
307 CD200R [69]. Several viruses, including cytomegalovirus [70] and herpesvirus [71] manipulated the
308 CD200-CD200R pathway as a means of immune evasion. Interestingly, in one of the longest
309 running and most in-depth studies of host-pathogen coevolution, CD200R was shown to be under
310 selection in rabbits in response to myxoma virus biocontrol agent [72]. As DFT1 and DFT2 have
311 been circulating in devils for more than 20 years and 5 years, respectively, it will be important to
312 monitor CD200/R expression and the potential evolution of paired activating and inhibitory
313 receptors in these natural disease models [73].

314 Immunophenotyping and single-cell RNAseq of circulating tumor cells (CTCs) has
315 potential to identify key gene expression patterns associated with metastasis and tissue invasion.
316 Periaxin (PRX) is the most sensitive and specific marker for DFT1 cells in immunohistochemistry
317 assays [74]. Unfortunately, PRX is expressed primarily in the cytoplasm, which eliminates the
318 possibility of using PRX as a marker to sort live cells via flow cytometry for single-cell RNAseq.
319 However, CD200 is a potential marker for the identification of circulating tumor cells (CTCs) from
320 devil blood. As proof of concept, DFT2 cells could be identified in devil blood spiked with DFT2
321 cells. As CTCs are likely to be rare in the blood of most infected devils, CD200 alone would be
322 insufficient for identifying DFT1 cells. Additional surface DFT markers would be required to
323 purify CTCs for metastases and tissue invasion analyses. The FAST protein system provides a
324 simple procedure to facilitate the production of a panel of DFT-markers to help identify key
325 proteins in the metastatic process.

326 In summary, the simple "cut-and-paste" production of the vectors and single-step testing
327 pipeline of the FAST system provided multiple benefits. The FAST system allowed us to
328 characterize receptor-ligand interactions, and to identify evolutionarily conserved immune evasion
329 pathways in naturally occurring transmissible cancers. Our initial implementation of the system
330 confirmed numerous predicted protein interactions for the first time in a marsupial species and
331 documented high expression of the inhibitory molecule CD200 on DFT cells. The high expression
332 of CD200 in devil nervous tissues and neuroendocrine tumors, downregulation of CD200 in
333 response to imiquimod, and binding of CD200 to CD200R1, is consistent with results from human
334 and mouse studies. Consequently, the CD200/R pathway provides a promising immunotherapy
335 and vaccine target for DFTs. Beyond this study, FAST proteins meet the key attributes needed for
336 reagent development, such as being straightforward to make, stable, versatile, renewable, cheap,

337 and amenable to high-throughput testing [75]. The direct fusion of the reporter protein to the protein-
338 of-interest allows for immediate feedback during transfection, supernatant testing, and protein
339 purification; proteins with frameshifts, introduced stop codons, or folded improperly will not
340 fluoresce and can be discarded after a simple visualization, rather than only after extensive
341 downstream testing. Efficient mapping of immune checkpoint interactions across species can
342 identify evolutionarily conserved immune evasion pathways and appropriate large animal models
343 with naturally occurring cancer. This knowledge could inform veterinary and human medicine in
344 the fields of immunological tolerance to tissue transplants, infectious disease, and cancer.
345

346 **MATERIALS AND METHODS**

347 **Study design**

348 The objectives of this study were to fill a major gap in our understanding of the mammalian
349 immune system and to understand how genetically mismatched transmissible tumors evade host
350 immunity. To achieve this goal, we developed a recombinant protein system that directly fuses
351 proteins-of-interest to a fluorescent reporter protein. The first phase was to determine if the
352 fluorescent protein remained fluorescent after secretion from mammalian cells and to confirm that
353 proteins bound to their predicted receptors (i.e. ligands). Initial testing was performed in CHO
354 cells and follow-up assays used devil cells. To further demonstrate the functionality of this system
355 for antibody development, mice were immunized with either 41BB or CD200 proteins. Pre- and
356 post-immunization polyclonal sera was used to confirm that the proteins used for immunization
357 induced antibodies that specifically bound to surface-expressed recombinant proteins and native
358 proteins on devil facial tumor cells.

359 **Target transcript amplification**

360 Target gene DNA sequences for vector construction were retrieved from Genbank,
361 Ensembl or de novo transcriptome assemblies (**Table S2**) [76]. Target DNA was amplified from a
362 cDNA template or existing plasmids using primers and PCR conditions shown in **Tables S2-S4**
363 using Q5 High-Fidelity 2X Master Mix (New England Biolabs # M0494L). Primers were ordered
364 with 5' base extensions that overlapped expression vectors on either side of the restriction sites.
365 The amplified products were identified by gel electrophoresis and purified using Nucleospin PCR
366 and Gel Clean Up Kit (Macherey-Nagel # 740609.5). Alternatively, DNA sequences were
367 purchased as double stranded DNA gblocks (**Table S5**) (Integrated DNA Technologies) for direct
368 assembly into expression vectors.

369 **Construction of all-in-one Sleeping Beauty transposon vectors**

370 All new plasmids were assembled using NEBuilder kit (NEB # E5520S) following the
371 manufacturer's recommendations unless otherwise noted. DNA inserts, digested plasmids, and
372 NEBuilder master mix were incubated for 60 minutes at 50 °C and then transformed into DH5α
373 included with the NEBuilder kit. Plasmid digestions were performed following manufacturer
374 recommendations and generally subjected to Antarctic phosphatase (New England Biolabs #
375 M0289S) treatment to prevent potential re-annealing. Sleeping Beauty transposon vectors pSBbi-
376 Hyg (Addgene # 60524), pSBbi-BH (Addgene # 60515), pSBtet-Hyg (Addgene # 60508), pSBtet-
377 RH (Addgene # 60500) were gifts to Addgene from Eric Kowarz [77]. The pCMV(CAT)T7-SB100
378 containing the CMV promoter and SB100X transposase was a gift to Addgene from Zsuzsanna
379 Izsvak (Addgene # 34879) [78]. We first constructed an all-in-one Sleeping Beauty vector by
380 inserting a CMV promoter and SB100X transposase from pCMV(CAT)T7-SB100 [78] into pSBi-
381 BH [77] (**Tables S3-S4**). This was accomplished by using pAF111-vec.FOR and pAF111.1.REV
382 primers to amplify an overlap region from pSBbi-BH (insert 1) and pAF111-2.FOR and pAF111-

383 2.REV to amplify the CMV-SB100X region from pCMV(CAT)T7-SB100 (insert 2). The purified
384 amplicons were then used for NEBuilder assembly of pAF111. The final all-in-one vectors
385 pAF112 (hygromycin resistance and luciferase) and pAF123 (hygromycin resistance) were
386 assembled from the pAF111 components. pAF112 was assembled by amplifying the Luc2
387 luciferase gene (insert 1) from pSBtet-Hyg and the P2A-hygromycin resistance gene (insert 2)
388 from pSBbi-BH and inserting into the pAF111 Bsu36I digest using NEBuilder. pSBbi-Hyg was
389 Bsu36I-digested to obtain the hygromycin resistance gene, and this fragment was inserted into
390 Bsu36I-digested pAF111 using T4 ligase cloning to replace the BFP-P2A-hygromycin segment in
391 pAF111.

392 **Construction of full-length protein vectors**

393 All full-length gene coding sequences except CTLA4 were cloned into the a pAF112 SfiI
394 digest (**Table S2**). All full-length vectors also contain luciferase with T2A peptide linked to the
395 hygromycin resistance protein; luciferase was included for use in downstream functional testing
396 that was not part of this study. Tasmanian devil CTLA4 was cloned into a NotI-HF and XmaI
397 digest of pAF100 that was used in a different study but is derived from vectors pAF112 and
398 pAF138. Additionally, we also used devil PDL1 (CHO.pAF48) and 41BBL (CHO.pAF56) cell
399 lines developed using a vector system described previously [25].

400 **Construction of FAST protein vectors**

401 Plasmids containing fluorescent protein coding sequences mCerulean3-N1 (Addgene #
402 54730), mAzurite-N1 (Addgene # 54617), mOrange-N1 (Addgene # 54499), mNeptune2-N1
403 (Addgene # 54837) were gifts to Addgene from Michael Davidson. mTag-BFP was amplified from
404 pSBbi-BH, mCitrine was amplified from pAF71, and mCherry was amplified from pTRE-Dual2
405 (Clontech # PT5038-5). pAF137 was constructed by amplifying the devil 41BB extracellular

406 domain with primers pAF137-1.FOR and pAF137-1.REV and amplifying mCherry with pAF137-
407 2a.FOR and pAF137-2.REV (**Table S3-4**). 5' extensions on pAF137-1.FOR and pAF137-2.REV
408 were used to create overlaps for NEBuilder assembly of pAF137 from a pAF123 SfiI-digested
409 base vector. 3' extensions on pAF137-1.REV and pAF137-2a.FOR were used to create the linker
410 that included an XmaI/SmaI restriction site, TEV cleavage tag, GSAGSAAGSGEF linker peptide,
411 and 6x-His tag between the gene-of-interest and fluorescent reporter. The GSAGSAAGSGEF was
412 chosen due to the low number of large hydrophobic residues and less repeated nucleic acids than
413 are needed with other flexible linkers such as $(GGGS)_4$ [79]. The pAF137 primer extensions also
414 created 5' NotI and 3' NheI sites in the FAST vector to facilitate downstream swapping of
415 functional genes and to create a Kozak sequence [80] (GCCGCCACC) upstream of the FAST protein
416 open-reading frame. Following confirmation of correct assembly via DNA sequencing, the FAST
417 41BB-mCherry (pAF137) was digested and used as the base vector (**Figure 2B** and **Figure S1A-**
418 **B**) for development of FAST vectors with alternative fluorescent proteins. This was accomplished
419 by digestion of pAF137 with SalI and NheI and then inserting PCR-amplified coding sequences
420 for other fluorescent proteins using NEBuilder (**Tables S3-S4**).

421 Type I FAST (extracellular N-terminus, cytoplasmic C-terminus) protein vectors were
422 constructed by digestion of 41BB FAST vectors with NotI and either XmaI or SmaI (**Figure 2B**
423 and **Figure S1A-B**), and then inserting genes-of-interest (**Tables S2-4**). To create an Fc-tagged
424 FAST protein we fused the extracellular domain of devil CD80 to the Fc region of the devil IgG
425 (**Figure S1C**). The Fc region was amplified from a devil IgG plasmid provided by Lynn Corcoran
426 (Walter and Eliza Hall Institute of Medical Research). All secreted FAST proteins in this study
427 used their native signal peptides, except for 41BBL. 41BBL is a type II transmembrane protein in
428 which the signal peptide directly precedes the cytoplasmic and transmembrane domains of the

429 protein (cytoplasmic N-terminus, extracellular C-terminus). As type I FAST vectors cannot
430 accommodate this domain architecture, we developed an alternative base vector for type II
431 transmembrane FAST proteins (**Figure S1D**). To increase the probability of efficient secretion of
432 type II FAST proteins from CHO cells, we used the hamster IL-2 signal peptide (accession #
433 NM_001281629.1) at the N-terminus of the protein, followed by a SalI restriction site, mCherry,
434 an NheI restriction site, 6x-His tag, GSAGSAAGSGEF linker, TEV cleavage site, XmaI/SmaI
435 restriction site, the gene-of-interest, and a PmeI restriction site following the stop codon.

436 **General plasmid assembly, transformation, and sequencing**

437 Following transformation of assembled plasmids, colony PCR was performed as an initial
438 test of the candidate plasmids. Single colonies were inoculated directly into a OneTaq Hot Start
439 Quick-Load 2X Master Mix (NEB # M0488) with primers pSB_EF1a_seq.FOR
440 (atcttggttcattctcaagcctcag) and pSB_bGH_seq.REV (aggcacagtcgaggctgat). PCR was performed
441 with 60 °C annealing temperature for 25-35 cycles. Colonies yielding appropriate band sizes were
442 used to inoculate Luria broth with 100 µg/mL ampicillin for bacterial outgrowth overnight at 37
443 °C and 200 RPM. The plasmids were purified using standard plasmid kits and prepared for Sanger
444 sequencing using BigDye Terminator v3.1 Cycle Sequencing Kit (ThermoFisher # 4337455) with
445 pSB_EF1a_seq.FOR and pSB_bGH_seq.REV primers. The BigDye® Terminator was removed
446 using Agencourt CleanSEQ® (Beckman Coulter # A29151) before loading samples to an Applied
447 Biosystems® 3500XL Genetic Analyzer (Applied Biosystems) for sequencing by fluorescence-
448 based capillary electrophoresis.

449 **General cell culture conditions**

450 DFT1 cell line C5065 and DFT2 cell line JV were cultured at 35 °C with 5% CO_2 in cRF10
451 (10% complete RPMI (Gibco # 11875-093) with 2 mM L-glutamine, supplemented with 10% heat-

452 inactivated fetal bovine serum (FBS), and 1% antibiotic-antimycotic (ThermoFisher # 15240062).
453 RPMI without phenol red (Sigma # R7509) was used to culture FAST protein cell lines when
454 supernatants were collected for downstream flow cytometry assays. Devil peripheral blood cells
455 were cultured in cRF10 at 35 °C with 5% CO_2. CHO cells were cultured at 37 °C in cRF10 during
456 transfections and drug selection but were otherwise cultured at 35 °C in cRF5 (5% complete
457 RPMI). For production of purified recombinant proteins, stably transfected CHO cells were
458 cultured in suspension in spinner flasks in chemically defined, serum-free CHO Ex-Cell (Sigma #
459 14361C) media supplemented with 8 mM L-glutamine, 10 mM HEPES, 50 μM 2-ME, 1% (v/v)
460 antibiotic-antimycotic, and 1 mM sodium pyruvate and without hygromycin.

461 **Transfection and Generation of Recombinant Cell Lines**

462 Stable transfections of CHO and DFT cells were accomplished by adding 3 x 10^5 cells to
463 each well in 6-well plates in cRF10 and allowing the cells to adhere overnight. The next day, 2 μg
464 of plasmid DNA was added to 100 μL of PBS in microfuge tubes. Polyethylenimine (PEI) (linear,
465 MW 25,000; Polysciences # 23966-2) was diluted to 60 μg/mL in PBS and incubated for at least
466 two minutes. 100 μL of the PEI solution was added to the 100 μL of plasmid DNA in each tube to
467 achieve a 3:1 ratio of PEI:DNA. The solution was mixed by gentle pipetting and incubated at room
468 temperature for 15 minutes. Whilst the solution was incubating, the media on the CHO cells were
469 replaced with fresh cRF10. All 200 μL from each DNA:PEI mix was then added dropwise to the
470 CHO cells and gently rocked side-to-side and front-to-back to evenly spread the solution
471 throughout the well. The plates were then incubated overnight at 37 °C with 5% CO_2. The next
472 day the plates were inspected for fluorescence and then the media was removed and replaced with
473 cRF10 containing 1 mg/mL hygromycin (Sigma # H0654). The media was replaced with fresh
474 cRF10 1 mg/ml hygromycin every 2-3 days for the next seven days until selection was complete.

475 The cells were then maintained in 0.2 mg/mL hygromycin in cRF5 at 35 °C with 5% CO_2.
476 Supernatant was collected 2-3 weeks post-transfection and stored at 4 °C for two months to assess
477 stability of secreted FAST proteins.

478 **Protein production and purification**

479 16 days post-transfection the first batch of FAST protein cell lines were adapted to a 1:1
480 mix of cRF5 and chemically defined, serum free CHO Ex-cell media for 1-2 days to facilitate
481 adaptation of the adherent CHO cells to suspension culture in serum-free media. At least $5x10^7$
482 cells were then transferred to Proculture spinner flasks (Sigma # CLS45001L, CLS4500250) and
483 stirred at 75 RPM at 35 °C in 5% CO_2 on magnetic stirring platforms (Integra Bioscience #
484 183001). Cells were maintained at a density ranging from $5x10^5$ to $2x10^6$ cells/ml for 8-14 days.
485 Supernatant was collected every 2-3 days, centrifuged at 3200 RCF for 10 minutes, stored at 4 °C,
486 and then purified using the ÄKTA start protein purification system (GE Life Sciences #
487 29022094). The supernatant was diluted 1:1 with 20 mM sodium phosphate pH 7.4 and then
488 purified using HisTrap Excel columns (GE Life Sciences # 17-3712-05) according to the
489 manufacturer's instructions. Samples were passed through the columns using a flow rate of 2
490 mL/minute at 4 °C; all wash and elution steps were done at 1 mL/minute. Elution from HisTrap
491 columns (GE Life Sciences # 17-3712-05) was accomplished using 0.5 M imidazole and
492 fractionated into 1 ml aliquots using the Frac30 fraction collector (GE Life Sciences # 29023051).
493 Fluorescence of FAST proteins was checked via brief excitation (**Figure 2D**) on a blue light
494 transilluminator with an amber filter unit. In the case of mCherry chromogenic color was visible
495 (**Figure 2E**) without excitation. Fractions containing target proteins were combined and diluted to
496 15 mL with cold PBS, dialyzed (Sigma # PURX60005) in PBS at 4 °C, 0.22 μm sterile-filtered
497 (Millipore # SLGV033RS) and concentrated using Amicon Ultra centrifugal filter units (Sigma #

498 Z706345). The protein concentration was quantified using the 280 nm absorbance on a Nanodrop
499 spectrophotometer. Extinction coefficients using for each protein were calculated using the
500 ProtParam algorithm [81]. The proteins were then aliquoted into microfuge tubes and frozen at -80
501 °C until further use. The CTLA4-Fc-mCherry protein was designed, assembled, and tested
502 separately from the other FAST proteins and was tested directly in supernatant without
503 purification.

504 **Preparation of CHO cells expressing full-length proteins for flow cytometry**

505 CHO cells expressing full-length proteins were thawed in cRF10 and then maintained in
506 cRF5 with 0.2 mg/mL hygromycin. The adherent CHO cells were washed with PBS and incubated
507 with trypsin for 5 minutes at 37 °C to remove cells from the culture flask. Trypsin was diluted 5X
508 with cRF5 and centrifuged at 200 RCF for 5 minutes. Cells were resuspended in cRF5, counted
509 (viability > 95% in all cases), and resuspended and aliquoted for assays as described below.

510 **Initial staining of CHO cells with 41BB FAST protein supernatants (without chloroquine)**

511 Supernatants (cRF5) were collected from CHO cells expressing devil 41BB-extracellular
512 domain fused to either mCherry (pAF137), mCitrine (pAF138), mOrange (pAF164), mBFP
513 (pAF139), mAzurite (pAF160), mCerulean3 (pAF161), or mNeptune2 (pAF163) (**Tables S2-4**).
514 The supernatant was spun for 10 minutes at 3200 RCF to remove cells and cellular debris, and
515 then stored at 4 °C until further use. CHO cells expressing devil 41BBL (CHO.pAF56) and
516 untransfected CHO cells were prepared as described above. Flow cytometry tubes were loaded
517 with 5 x 10^4 target CHO cells/well in cRF5, centrifuged 500 RCF for 3 minutes, and then
518 resuspended in 200 µL of supernatant from the 41BB FAST cell lines (n=1/treatment). The tubes
519 were then incubated for 15 minutes at 4 °C, centrifuged at 500 RCF for 3 minutes, resuspended in
520 400 µL of cold FACS buffer, and stored on ice until the data were acquired on a Beckman-Coulter

521 Astrios flow cytometer (**Figure 2C**). All flow cytometry data was analyzed using FCS Express 6
522 Flow Cytometry Software version 6 (Denovo Software).

523 **Staining CHO cells with FAST protein supernatants (without chloroquine)**

524 U-bottom 96-well plates were loaded with 1 x 10^5 target CHO cells/well in cRF5,
525 centrifuged 500 RCF for 3 minutes, and then resuspended in 175 µL of cRF5 supernatant from
526 FAST cell lines collected 11 days after transfection (n=1/treatment). The plates were then
527 incubated for 30 minutes at room temperature, centrifuged at 500 RCF for 3 minutes, resuspended
528 in 200 µL of cold FACS buffer, centrifuged again and fixed with FACS fix buffer (PBS, 0.02%
529 NaN3, 0.4% formalin, 10g/L glucose). The cells were transferred to tubes, diluted with FACS
530 buffer and analyzed on a Beckman-Coulter Astrios flow cytometer (**Figure S2**).

531 **Staining CHO cells with purified FAST proteins (with chloroquine)**

532 Purified FAST proteins were diluted to 20 µg/mL in cRF5, aliquoted into V-bottom 96-
533 well transfer plates, and then stored at 37 °C until target cells were ready for staining. Target cells
534 were resuspended in cRF5 with 100 µM chloroquine and 100,000 cells/well were aliquoted into
535 U-bottom 96-well plates. 100 µL of the diluted FAST proteins (n=1/treatment, 2
536 timepoints/treatment) were then transferred from the V-bottom plates into the U-bottom 96-well
537 plates containing target cells. The final volumes and concentrations were 200 µL/well in cRF5
538 with 50 µM chloroquine and 2 µg/well of FAST proteins. One set of plates was incubated at 37 °C
539 for 30 minutes and another set of plates was incubated at 37 °C overnight. The cells were then
540 centrifuged 500 RCF for 3 minutes, the media decanted, and incubated for 5 minutes with 100 µL
541 of trypsin to dislodge adherent cells. The cells were then washed with 200 µL of cold FACS buffer,
542 fixed, resuspended in cold FACS buffer, and transferred to tubes for analysis on the Astrios flow
543 cytometer (**Figure 3B**).

544 **Staining CHO cells with FAST supernatants (with chloroquine)**

545 The protocol for using FAST protein supernatants was the same above as the preceding
546 experiment except for the modifications described here. Supernatants were collected 2-3 weeks
547 post-transfection, centrifuged at 3200 RCF for 10 minutes, and stored at 4 °C for 2 months. Prior
548 to staining for flow cytometry, the supernatant was 0.22 µm filtered. Supernatant was then loaded
549 into V-bottom 96-well plates to facilitate rapid transfer to staining plates and stored at 37 °C until
550 target cells were ready for staining. Target cells were prepared as described above except for being
551 diluted in cRF5 with 100 µM chloroquine. 2 x 10^5 cells/well (100 µL) were then loaded into U-
552 bottom 96-well plates. 100 µL of FAST protein supernatant (n=1/treatment) was then transferred
553 from the V-bottom plates to achieve 50 µM chloroquine and the cells were then incubated at 37
554 °C for 60 minutes. The plates were then washed, fixed, and analyzed on the Astrios flow cytometer
555 (**Figure S3**). A similar procedure was used for staining stably-transfected DFT cells with CTLA4-
556 Fc-mCherry, except that the supernatant was used fresh (**Figure 4D**).

557 **Coculture assay with full-length target and FAST protein CHO cell lines (with chloroquine)**

558 CHO cells expressing full-length CTLA4 with a C-terminal mCitrine, and CHO cells
559 expressing full-length 41BB or 41BBL were labelled with 5 µM CFSE; CFSE and mCitrine were
560 analyzed using the same excitation laser (488 nm) and emission filters (513/26 nm). 1 x 10^5 FAST
561 protein-secreting cells were mixed with 1 x 10^5 target cells in cRF5 with 50 µM chloroquine and
562 incubated overnight at 37 °C in 96-well U-bottom plates (**Figure 4A)**. The next day the cells were
563 rinsed with PBS, trypsinized, washed, fixed, and resuspended in FACS buffer prior to running
564 flow cytometry. Cells were gated on forward and side scatter (FSC x SSC) and for singlets (FSC-
565 H x FSC-A). (**Figure 4B).** Data shown in **Figure 4C** is representative of n=3 technical

566 replicates/treatment. Data was collected using a Beckman Coulter MoFlo Astrios and analyzed
567 using FCS Express.

568 **Analysis of checkpoint molecule expression in DFT cells and Tasmanian devil tissues**

569 RNAseq data was generated during previous experiments, aligned against the reference
570 Tasmanian devil genome Devil_ref v7.0 (GCA_000189315.1) and summarised into normalized
571 read counts as previously described [34,35]. RPKM-normalized read counts were produced in R using
572 edgeR[82]. Genes were ranked from highest RPKM-normalized count to lowest RPKM-normalized
573 count, and a heat map was produced for the genes of interest using the heatmap.2 function of
574 gplots. Heatmap color represents gene ranking among 18,788 predicted protein-coding genes in
575 the reference genome.

576 **Staining DFTs cell with CD200/R FAST proteins**

577 50,000 DFT cells/well were aliquoted into u-bottom 96-well plates, washed with 150 µL
578 of cRF10, and resuspended in 100 µL of warm cRF10 containing 100 µM chloroquine. 5 µg of
579 FAST protein/well was then added and mixed by pipetting. The plates were then incubated at 37
580 °C for 30 minutes. The cells were then transferred to microfuge tubes without washing, stored on
581 ice, and analyzed on a Beckman Coulter MoFlo Astrios (n=2/treatment).

582 **Polyclonal antibody development**

583 CD200 and 41BB FAST proteins were digested overnight with TEV protease (Sigma #
584 T4455) at 4 °C in PBS. The cleaved linker and 6x-His tag were then removed using a His SpinTrap
585 kit (GE Healthcare # 28-9321-71). Digested proteins in PBS were diluted 1:1 in Squalvax (Oz
586 Biosciences # SQ0010) to a final concentration of 0.1 µg/µL and was mixed using interlocked
587 syringes to form an emulsion. Immunization of BALB/c mice for antibody production was
588 approved by the University of Tasmania Animal Ethics Committee (# A0014680). Pre-immune

589 sera were collected prior to subcutaneous immunization with at least 50 μL of the emulsion. On
590 day 14 post-immunization the mice were boosted using a similar procedure. On day 50 the mice
591 received a booster with proteins in IFAVax (Oz Biosciences # IFA0050); mice immunized with
592 CD200 again received subcutaneous injections, whereas 41BB mice received subcutaneous and
593 intraperitoneal injections. Pre-immune and sera collected after 3X immunizations were then tested
594 by flow cytometry against CHO cells expressing either 41BB or CD200. CHO cells were prepared
595 as described above and $2x10^5$ cells were incubated with mouse serum diluted 1:200 in PBS for 30
596 minutes at 4 °C. The cells were then washed 2X and stained with 50 μL of anti-mouse IgG
597 AlexaFluor 647 diluted 1:1000 in FACS buffer. The cells were then washed 2X, stained with DAPI
598 to identify live cells, and analyzed on a Cyan ADP flow cytometer (**Figure 5C**). CD200 and 41BB
599 expression on DFT cells was tested using a procedure similar to the CHO cell staining, except the
600 sera used was collected after 4X immunizations and was diluted 1:500 and analyzed on the BD
601 FACSCanto II (**Figure 5D**).

602 **Purification of antibodies from normal mouse serum (NMS) and anti-CD200 serum**

603 Approximately 200 μL of normal mouse serum or anti-CD200 serum day 157 (after 4X
604 immunizations) were purified using a protein G SpinTrap (GE Healthcare # 28-4083-47) according
605 to the manufacturer's instrutions. Serum was diluted 1:1 with 20 mM sodium phosphate, pH 7.0
606 binding buffer, eluted with 0.1 M glycine-HCl, pH 2.7, and the pH was neutralized with 0.1 M
607 glycine-HCl, pH 2.7. The eluted antibodies were then concentrated using an Amicon Ultra 0.5
608 centrifugal until (Merck # UFC500308) by centrifuging at 14,000 RCF for 30 minutes at 4 °C and
609 then washing the antibodies with 400 μL of PBS twice. The protein concentration was then
610 quantified on a Nanodrop spectrophotometer at 280 nm using the extinction coefficients for IgG.

611 **Testing CD200 expression on DFT cells that overexpress CD200R1**

612 50,000 DFT cells/well were aliquoted into u-bottom 96-well plates and washed with 200
613 μL of cold FACS buffer. Purified polyclonal anti-CD200 was diluted to 2.5 μg/mL in cold FACS
614 buffer and the cells in appropriate wells were resuspend in 100 μL/well (0.25 μg/well) diluted
615 antibody; wells that did not receive antibody were resuspended in 100 μL of FACS buffer. The
616 cells were incubated on ice for 20 minutes and then washed with 200 μL of FACS buffer. Whilst
617 incubating, anti-mouse IgG-AF647 was diluted to 1 μg/mL in cold FACS buffer and then used to
618 resuspend cells in the appropriate wells. The plates were incubated on ice for 20 minutes, then
619 washed with 100 μL of cold FACS buffer. The cells were then resuspended in 200 μL of FACS
620 fix and incubated on a rocking platform at room temp for 15 minutes. The cells were then
621 centrifuged 500 RCF for 3 minutes at 4 °C, resuspended in 200 μL FACS buffer and stored at 4
622 °C until they were analyzed on a FACSCanto II (n=2/treatment).

623 **Isolation of devil peripheral blood mononuclear cells**

624 Blood collection from Tasmanian devils was approved by the University of Tasmania
625 Animal Ethics Committee (permit # A0014599) and the Tasmanian Department of Primary
626 Industries, Parks, Water and Environment (DPIPWE). Blood was collected from the jugular vein
627 and stored in EDTA tubes for transport to the lab. Blood was processed within three hours by
628 diluting 1:1 with serum-free RPMI and then layering onto Histopaque (Sigma # 10771) before
629 centrifuging at 400 RCF for 30 minutes. The interface containing the peripheral blood
630 mononuclear cells was then collected using a transfer pipette, diluted with 50 mL of serum-free
631 RPMI and centrifuged for 5 minutes at 500 RCF. Cells were washed with again with cRF10 and
632 then either used fresh or stored at -80 °C until further use.

633 **Detecting DFT2 cells in PBMC using CD200**

634 Frozen devil PBMC were thawed and cultured in cRF10 at 35 °C with 5% CO_2 for 2 hours,
635 cells were then washed in FACS buffer, counted and $3x10^5$ PBMC cells used per sample. DFT2.JV
636 cells were removed from culture flasks, counted, and $2x10^5$ cells used per sample. Samples were
637 incubated with 50 µL normal goat serum (Thermo Cat # 01-6201) diluted 1:200 in FACS buffer
638 for 15 minutes at 4 °C, 50 µL of anti-CD200 serum diluted 1:100 was added (1:200 final) for 30
639 minutes at 4 °C. Cells were then washed 2X and stained with 50 µL of anti-mouse IgG AlexaFluor
640 647 diluted to 1 µg/mL in FACS buffer for 30 minutes at 4 °C. The cells were then washed 2X,
641 stained with DAPI (Sigma Cat # D9542) to identify live cells, and analyzed on the BD FACSCanto
642 II. PBMC and DFT cells were run separately then PBMC and DFT2 mixed at a ratio of 10:1 by
643 volume for the combined samples (n=1/treatment) (**Figure S4A**). The experiment was repeated
644 (n=1/treatment), except that PBMCs and DFT cells were mixed at a 5:1 ratio (**Figure S4B**).

645 **Staining of DFT cells in devil whole blood**

646 DFT1.C5065 and DFT2.JV cells were labelled with 5 µM CellTrace violet (CTV) and
647 cultured for three days at 37 °C. On the day of the assays peripheral blood from one devil was
648 collected and stored at ambient temp for less than three hours. 100 µL of whole blood was aliquoted
649 into 15 mL tubes and stored at ambient temperature whilst DFT cells were prepared. The media
650 on CTV-labeled DFT cells were decanted and the cells were detached from the flask by incubating
651 in 2.5 mL of TrypLE Select for 5 minutes at 37 °C. The cells were washed with cRF10,
652 resuspended in cRF10, and counted. DFT cells were then diluted to $1x10^4$ cells/mL in cRF10 and
653 100 µL were aliquoted into appropriate 15 mL tubes containing 100 µL of whole blood. 1 µL of
654 purified anti-CD200 (0.5 µg/tube) was diluted into the appropriate tubes and incubated for 15
655 minutes at ambient temperature. Next, 0.5 µg/tube of anti-mouse IgG AF647 was added to each
656 tube. Note: 0.5 µL (0.5 µg) of concentrated secondary antibody was accidentally added directly to

657 the tube for the data shown in the top row and middle column of **Figure S5A;** for all other tubes
658 the secondary antibody was diluted 1:20 in PBS and 10 µL was added to each tube. The cells were
659 then incubated for 15 minutes at ambient temperature. The cells were then diluted in 1 mL
660 ammonium chloride red blood cell (RBC) lysis buffer (150 mM NH_4Cl, 10 mM $KHCO_3$, 0.1 mM
661 EDTA disodium (Na_2-$2H_2O$)) and mixed immediately gently pipetting five times. The cells were
662 incubated at ambient temperature for 10 minutes and then diluted with 5 mL of PBS and
663 centrifuged 500 RCF for 3 minutes. Some tubes contained residual RBCs, so the pellet was
664 vigorously resuspended in 5 mL of RBC lysis buffer, incubated for 5 minutes, diluted with 5 mL
665 of cold FACS buffer, and centrifuged 500 RCF for 3 minutes. The cells were then resuspended in
666 250 µL of FACS buffer and stored on ice until analysis on a Beckman Coulter MoFlo Astrios
667 (n=1/treatment). Data were analyzed in FCS Express version 6 (**Figure S5**).

668 The experiment above was repeated with the following modifications. DFT cells were
669 labelled with 5 µM of CFSE and incubated for two days at 37 °C. On the day of the assays fresh
670 blood was collected from two devils. Purified anti-CD200 and NMS were labeled with Zenon
671 mouse IgG AF647 (ThermoFisher # Z25008) and blocked with the Zenon blocking agent. $1x10^4$
672 CFSE-labeled DFT cells were diluted directly into 100 µL of whole blood in 15 mL tubes and 12
673 µL (2 µL antibody, 5 µL labeling agent, 5 µL blocking agent) of Zenon AF647-labeled purified
674 NMS or anti-CD200 were added directly to the cells. The cells were incubated for 30 minutes at
675 ambient temperature. The cells were then gently resuspended in 2.5 mL of RBC lysis buffer and
676 incubated for 10 minutes at ambient temperature. The cells were diluted with 10 mL of PBS and
677 centrifuged 500 RCF for 3 minutes. The cells were resuspended in 1.5 mL of RBC lysis buffer and
678 incubated for another 10 minutes to lyse residual RBCs. The tubes were then resuspended in 9 mL
679 of cRF10 and centrifuged 500 RCF for 3 minutes. The cells were resuspended in 350 µL of cold

680 FACS buffer containing 200 ng/mL of DAPI and stored on ice until analysis on a Beckman Coulter
681 MoFlo Astrios (n=1/treatment for n = 2 devils) (**Figure 6**).
682

683 **ACKNOWLEDGMENTS**

684 We wish to thank Ginny Ralph for her ongoing care of Tasmanian devils, and the Bonorong
685 Wildlife Sanctuary for providing access to Tasmanian devils, and Ruth Pye for providing care for
686 devils and collecting blood samples. We would like to thank John Hayball and Georgina
687 Kalodimos for advice and assistance, Mahalia Kingsley and Nirdesh Poudel for plasmid
688 construction, Nick Blackburn for bioinformatics assistance, Lynn Corcoran for the devil IgG
689 plasmid, James Murphy for a devil IL-15 plasmid, Emily Flies for editing the manuscript, and
690 Kay Holekamp for her comments on the manuscript. **Funding:** ARC DECRA grant #
691 DE180100484, ARC Linkage grant # LP0989727, ARC Discovery grant # DP130100715, Morris
692 Animal Foundation Grant-in-Aid # D14ZO-410, University of Tasmania Foundation Dr Eric
693 Guiler Tasmanian Devil Research Grant through funds raised by the Save the Tasmanian Devil
694 Appeal (2013, 2015, 2017, 2018), and Entrepreneurs' Programme - Research Connections grant
695 with Nexvet Australia Pty. Ltd. # RC50680.
696

697 **AUTHOR CONTRIBUTIONS**

698 ASF designed the study; ALP, ASF, CEBO, PRL, and PRM developed the technology; ASF,
699 CEBO, PRL, PRM, JMD, and TLP performed the experiments; ALP performed bioinformatic
700 analyses; ALP, ASF, JMD and PRL created the figures; ALP, ASF, PRL, JMD, TLP, and GMW
701 analyzed the data; ASF wrote the manuscript and all authors edited the manuscript.
702

703 **AVAILABILITY OF DATA AND MATERIALS**

704 All data are included with the paper. The FAST base vectors (pAF92.3 pAF112.7, pAF123.1,
705 pAF137.4c1, pAF138.7, pAF139.2, pAF160.1, pAF161.3, pAF163.1, pAF164.3) will be available
706 through Addgene (deposit # 77504).

707

708 **CONFLICT OF INTEREST**

709 The authors received funding from Nexvet Australia Pty. Ltd for related studies.

710

711 **REFERENCES**

712 1 Albuquerque TAF, Drummond do Val L, Doherty A, de Magalhães JP. From humans to
713 hydra: patterns of cancer across the tree of life. *Biol Rev* 2018; **93**: 1715–1734.
714 2 Abu-Helil B, Van Der Weyden L. Metastasis in the wild: investigating metastasis in non-
715 laboratory animals. *Clin Exp Metastasis* 2019. doi:10.1007/s10585-019-09956-3.
716 3 Olds JE, Burrough ER, Fales-Williams AJ, Lehmkuhl A, Madson D, Patterson AJ *et al.*
717 Retrospective Evaluation of Cases of Neoplasia in a Captive Population of Egyptian Fruit
718 Bats (Rousettus Aegyptiacus). *J Zoo Wildl Med* 2015; **46**: 325–332.
719 4 Chu PY, Zhuo YX, Wang FI, Jeng CR, Pang VF, Chang PH *et al.* Spontaneous neoplasms
720 in zoo mammals, birds, and reptiles in Taiwan - A 10-year survey. *Anim Biol* 2012; **62**:
721 95–110.
722 5 Deus A De, Alves F, Siqueira DB De, Rameh-de-albuquerque LC. Breast Carcinoma with
723 Pulmonary Metastasis in Armadillo (Eupharactus sexcinctus). *Acta Sci Vet* 2018; **46**: 1–5.
724 6 Kruse TN, Garner MM, Bonar CJ. A Retrospective Study of Pathologic Findings in
725 Captive Rock Hyrax (Procavia Capensis) in the United States. *J Zoo Wildl Med* 2015;
726 **46**: 798–805.
727 7 Effron M, Griner L, Benirschke K. Nature and rate of neoplasia found in captive wild
728 mammals, birds, and reptiles at necropsy. *J Natl Cancer Inst* 1977; **59**: 185–198.
729 8 Ratcliffe HL. Incidence and nature of tumors in captive wild mammals and birds. *Am J*
730 *Cancer* 1933; **17**: 116–135.
731 9 Priester WA, Mantel N. Occurrence of tumors in domestic animals. Data from 12 United
732 States and Canadian colleges of veterinary medicine. *J Natl Cancer Inst* 1971; **47**: 1333–
733 1344.

734 10 Howlader N, Noone A, Krapcho M, Miller D, Brest A, Yu M *et al.* SEER Cancer
735 Statistics Review, 1975-2016. Bethesda, MD, United States, 2016.
736 11 Griner LA. Neoplasms in Tasmanian devils (Sarcophilus harrisii). *J Natl Cancer Inst*
737 1979; **62**: 589–595.
738 12 Peck SJ, Michael SA, Knowles G, Davis A, Pemberton D. Causes of mortality and severe
739 morbidity requiring euthanasia in captive Tasmanian devils (Sarcophilus harrisii) in
740 Tasmania. *Aust Vet J* 2019; **97**: 89–92.
741 13 Pearse A-M, Swift K. Allograft theory: transmission of devil facial-tumour disease.
742 *Nature* 2006; **439**: 549.
743 14 Pye RJ, Pemberton D, Tovar C, Tubio JMC, Dun KA, Fox S *et al.* A second transmissible
744 cancer in Tasmanian devils. *Proc Natl Acad Sci* 2016; **113**: 374–379.
745 15 Murgia C, Pritchard JK, Kim SY, Fassati A, Weiss RA. Clonal Origin and Evolution of a
746 Transmissible Cancer. *Cell* 2006; **126**: 477–487.
747 16 Fleming JM, Creevy KE, Promislow DEL. Mortality in North American Dogs from 1984
748 to 2004: An Investigation into Age-, Size-, and Breed-Related Causes of Death. *J Vet*
749 *Intern Med* 2011; **25**: 187–198.
750 17 Lazenby BT, Tobler MW, Brown WE, Hawkins CE, Hocking GJ, Hume F *et al.* Density
751 trends and demographic signals uncover the long-term impact of transmissible cancer in
752 Tasmanian devils. *J Appl Ecol* 2018; **55**: 1368–1379.
753 18 James S, Jennings G, Kwon YM, Stammnitz M, Fraik A, Storfer A *et al.* Tracing the rise
754 of malignant cell lines: distribution, epidemiology and evolutionary interactions of two
755 transmissible cancers in Tasmanian devils. *Evol Appl* 2019; : eva.12831.
756 19 Siddle H V., Kreiss A, Tovar C, Yuen CK, Cheng Y, Belov K *et al.* Reversible epigenetic

757 down-regulation of MHC molecules by devil facial tumour disease illustrates immune
758 escape by a contagious cancer. *Proc Natl Acad Sci* 2013; **110**: 5103–8.
759 20 Yoshihama S, Roszik J, Downs I, Meissner TB, Vijayan S, Chapuy B *et al.* NLRC5/MHC
760 class I transactivator is a target for immune evasion in cancer. *Proc Natl Acad Sci* 2016;
761 **113**: 5999–6004.
762 21 Caldwell A, Coleby R, Tovar C, Stammnitz MR, Mi Kwon Y, Owen RS *et al.* The newly-
763 arisen devil facial tumour disease 2 (DFT2) reveals a mechanism for the emergence of a
764 contagious cancer. *Elife* 2018; **7**. doi:10.7554/eLife.35314.
765 22 Stammnitz MR, Coorens THH, Gori KC, Hayes D, Fu B, Wang J *et al.* The Origins and
766 Vulnerabilities of Two Transmissible Cancers in Tasmanian Devils. *Cancer Cell* 2018;
767 **33**: 607-619.e15.
768 23 Topalian SL, Hodi FS, Brahmer JR, Gettinger SN, Smith DC, McDermott DF *et al.*
769 Safety, Activity, and Immune Correlates of Anti–PD-1 Antibody in Cancer. *N Engl J Med*
770 2012; **366**: 2443–2454.
771 24 Larkin J, Chiarion-Sileni V, Gonzalez R, Grob JJ, Cowey CL, Lao CD *et al.* Combined
772 Nivolumab and Ipilimumab or Monotherapy in Untreated Melanoma. *N Engl J Med* 2015;
773 **373**: 23–34.
774 25 Flies AS, Bruce Lyons A, Corcoran LM, Papenfuss AT, Murphy JM, Knowles GW *et al.*
775 PD-L1 is not constitutively expressed on tasmanian devil facial tumor cells but is strongly
776 upregulated in response to IFN-γ and can be expressed in the tumor microenvironment.
777 *Front Immunol* 2016; **7**: 581.
778 26 Ong CEB, Lyons AB, Woods GM, Flies AS. Inducible IFN-γ Expression for MHC-I
779 Upregulation in Devil Facial Tumor Cells. *Front Immunol* 2018; **9**: 3117.

780 27 Flies AS, Blackburn NB, Lyons AB, Hayball JD, Woods GM. Comparative analysis of
781 immune checkpoint molecules and their potential role in the transmissible tasmanian devil
782 facial tumor disease. *Front Immunol* 2017; **8**: 513.
783 28 World Health Organization (WHO). WHO R&D Blueprint for action to prevent
784 epidemics. World Health Organization, 2016http://www.who.int/blueprint/en/ (accessed 1
785 May2018).
786 29 Shaner NC, Campbell RE, Steinbach PA, Giepmans BNG, Palmer AE, Tsien RY.
787 Improved monomeric red, orange and yellow fluorescent proteins derived from
788 Discosoma sp. red fluorescent protein. *Nat Biotechnol* 2004; **22**: 1567–72.
789 30 Cabantous S, Terwilliger TC, Waldo GS. Protein tagging and detection with engineered
790 self-assembling fragments of green fluorescent protein. *Nat Biotechnol* 2005; **23**: 102–
791 107.
792 31 Cha HJ, Dalal NN, Bentley WE. Secretion of human interleukin-2 fused with green
793 fluorescent protein in recombinant Pichia pastoris. *Appl Biochem Biotechnol* 2005; **126**:
794 1–11.
795 32 Duellman T, Burnett J, Yang J. Quantitation of secreted proteins using mCherry fusion
796 constructs and a fluorescent microplate reader. *Anal Biochem* 2015; **473**: 34–40.
797 33 Kammertoens T, Friese C, Arina A, Idel C, Briesemeister D, Rothe M *et al.* Tumour
798 ischaemia by interferon-γ resembles physiological blood vessel regression. *Nature* 2017;
799 **545**: 98–102.
800 34 Patchett AL, Wilson R, Charlesworth JC, Corcoran LM, Papenfuss AT, Lyons AB *et al.*
801 Transcriptome and proteome profiling reveals stress-induced expression signatures of
802 imiquimod-treated Tasmanian devil facial tumor disease (DFTD) cells. *Oncotarget* 2018;

803 **9**: 15895–15914.

804 35 Patchett AL, Coorens THH, Darby J, Wilson R, McKay MJ, Kamath KS *et al.* Two of a
805 kind: transmissible Schwann cell cancers in the endangered Tasmanian devil (Sarcophilus
806 harrisii). *Cell Mol Life Sci* 2019; : 1–12.

807 36 Seglen PO, Grinde B, Solheim AE. Inhibition of the Lysosomal Pathway of Protein
808 Degradation in Isolated Rat Hepatocytes by Ammonia, Methylamine, Chloroquine and
809 Leupeptin. *Eur J Biochem* 1979; **95**: 215–225.

810 37 Qureshi OS, Zheng Y, Nakamura K, Attridge K, Manzotti C, Schmidt EM *et al.* Trans-
811 endocytosis of CD80 and CD86: a molecular basis for the cell extrinsic function of
812 CTLA-4. *Science* 2011; **332**: 600–603.

813 38 van den Bremer ET, Beurskens FJ, Voorhorst M, Engelberts PJ, de Jong RN, van der
814 Boom BG *et al.* Human IgG is produced in a pro-form that requires clipping of C-terminal
815 lysines for maximal complement activation. *MAbs* 2015; **7**: 672–680.

816 39 Patchett AL, Latham R, Brettingham-Moore KH, Tovar C, Lyons AB, Woods GM. Toll-
817 like receptor signaling is functional in immune cells of the endangered Tasmanian devil.
818 *Dev Comp Immunol* 2015; **53**: 123–133.

819 40 Love JE, Thompson K, Kilgore MR, Westerhoff M, Murphy CE, Papanicolau-Sengos A
820 *et al.* CD200 Expression in Neuroendocrine Neoplasms. *Am J Clin Pathol* 2017; **148**:
821 236–242.

822 41 Murchison EP, Tovar C, Hsu A, Bender HS, Kheradpour P, Rebbeck CA *et al.* The
823 Tasmanian devil transcriptome reveals schwann cell origins of a clonally transmissible
824 cancer. *Science* 2010; **327**: 84–87.

825 42 Haile ST, Bosch JJ, Agu NI, Zeender AM, Somasundaram P, Srivastava MK *et al.* Tumor

826 cell programmed death ligand 1-mediated T cell suppression is overcome by coexpression
827 of CD80. *J Immunol* 2011; **186**: 6822–9.
828 43 Sugiura D, Maruhashi T, Okazaki I, Shimizu K, Maeda TK, Takemoto T *et al.* Restriction
829 of PD-1 function by *cis* -PD-L1/CD80 interactions is required for optimal T cell
830 responses. *Science* 2019; : eaav7062.
831 44 Moertel CL, Xia J, LaRue R, Waldron NN, Andersen BM, Prins RM *et al.* CD200 in CNS
832 tumor-induced immunosuppression: The role for CD200 pathway blockade in targeted
833 immunotherapy. *J Immunother Cancer* 2014; **2**: 46.
834 45 Challagundla P, Medeiros LJ, Kanagal-Shamanna R, Miranda RN, Jorgensen JL.
835 Differential Expression of CD200 in B-Cell Neoplasms by Flow Cytometry Can Assist in
836 Diagnosis, Subclassification, and Bone Marrow Staging. *AJCP / Orig Artic Am J Clin*
837 *Pathol* 2014; **142**: 837–844.
838 46 Spacek M, Karban J, Radek M, Babunkova E, Kvasnicka J, Jaksa R *et al.* CD200
839 Expression Improves Differential Diagnosis Between Chronic Lymphocytic Leukemia
840 and Mantle Cell Lymphoma. *Blood* 2014; **124**.
841 47 Saksena A, Yin CC, Xu J, Li J, Zhou J, Wang SA *et al.* CD23 expression in mantle cell
842 lymphoma is associated with CD200 expression, leukemic non-nodal form, and a better
843 prognosis. *Hum Pathol* 2019; **89**: 71–80.
844 48 Loh R, Hayes D, Mahjoor A, O'Hara A, Pyecroft S, Raidal S. The immunohistochemical
845 characterization of devil facial tumor disease (DFTD) in the Tasmanian Devil
846 (Sarcophilus harrisii). *Vet Pathol* 2006; **43**: 896–903.
847 49 Yao S, Zhu Y, Zhu G, Augustine M, Zheng L, Goode DJ *et al.* B7-h2 is a costimulatory
848 ligand for CD28 in human. *Immunity* 2011; **34**: 729–740.

849 50 Wang J, Sanmamed MF, Datar I, Su TT, Ji L, Sun J *et al.* Fibrinogen-like Protein 1 Is a
850 Major Immune Inhibitory Ligand of LAG-3. *Cell* 2018; **0**.
851 doi:10.1016/J.CELL.2018.11.010.
852 51 Aricescu AR, Lu W, Jones EY. A time- and cost-efficient system for high-level protein
853 production in mammalian cells. *Acta Crystallogr Sect D Biol Crystallogr* 2006; **62**: 1243–
854 1250.
855 52 Consortium SG, Biologiques A et F des M, Center BSG, Consortium CSG, Innovation IC
856 for S and F, Center ISP *et al.* Protein production and purification. *Nat Methods* 2008; **5**:
857 135.
858 53 Jayapal KP, Wlaschin KF, Hu WS, Yap MGS. Recombinant protein therapeutics from
859 CHO cells - 20 years and counting. *Chem Eng Prog* 2007; **103**: 40–47.
860 54 Atfy M. CD200 Suppresses the Natural Killer Cells and Decreased its Activity in Acute
861 Myeloid Leukemia Patients. *J Leuk* 2015; **3**.https://www.omicsonline.org/open-
862 access/cd200-suppresses-the-natural-killer-cells-and-decreased-its-activity-in-
863 acutemyeloid-leukemia-patients-2329-6917-1000190.pdf (accessed 18 Apr2019).
864 55 Coles SJ, Man S, Hills R, Wang EC, Burnett A, Darley RL *et al.* Over-Expression of
865 CD200 In Acute Myeloid Leukemia Mediates the Expansion of Regulatory T-
866 Lymphocytes and Directly Inhibits Natural Killer Cell Tumor Immunity. *Blood* 2015; **116**:
867 491.
868 56 Coles SJ, Wang ECY, Man S, Hills RK, Burnett AK, Tonks A *et al.* CD200 expression
869 suppresses natural killer cell function and directly inhibits patient anti-tumor response in
870 acute myeloid leukemia. *Leukemia* 2011; **25**: 792–9.
871 57 Gorczynski RM, Chen Z, Khatri I, Yu K. Graft-infiltrating cells expressing a CD200

872 transgene prolong allogeneic skin graft survival in association with local increases in
873 Foxp3 +Treg and mast cells. *Transpl Immunol* 2011; **25**: 187–193.
874 58 Gorczynski RM, Chen Z, He W, Khatri I, Sun Y, Yu K *et al.* Expression of a CD200
875 transgene is necessary for induction but not maintenance of tolerance to cardiac and skin
876 allografts. *J Immunol* 2009; **183**: 1560–1568.
877 59 Gorczynski L, Chen Z, Hu J, Kai Y, Lei J, Ramakrishna V *et al.* Evidence That an OX-2-
878 Positive Cell Can Inhibit the Stimulation of Type 1 Cytokine Production by Bone
879 Marrow-Derived B7-1 (and B7-2)-Positive Dendritic Cells. *J Immunol* 1999; **162**: 774–
880 781.
881 60 Harding J, Vintersten-Nagy K, Shutova M, Yang H, Tang JK, Massumi M *et al.* Induction
882 of long-term allogeneic cell acceptance and formation of immune privileged tissue in
883 immunocompetent hosts. Cold Spring Harbor Laboratory, 2019 doi:10.1101/716571.
884 61 Jenmalm MC, Cherwinski H, Bowman EP, Phillips JH, Sedgwick JD. Regulation of
885 Myeloid Cell Function through the CD200 Receptor. *J Immunol* 2014; **176**: 191–199.
886 62 Tovar C, Pye RJ, Kreiss A, Cheng Y, Brown GK, Darby J *et al.* Regression of devil facial
887 tumour disease following immunotherapy in immunised Tasmanian devils. *Sci Rep* 2017;
888 **7**: 43827.
889 63 Pye R, Patchett A, McLennan E, Thomson R, Carver S, Fox S *et al.* Immunization
890 strategies producing a humoral IgG immune response against devil facial tumor disease in
891 the majority of Tasmanian devils destined for wild release. *Front Immunol* 2018; **9**: 259.
892 64 Olin MR, Ampudia-Mesias E, Pennell CA, Sarver A, Chen CC, Moertel CL *et al.*
893 Treatment combining CD200 immune checkpoint inhibitor and tumor-lysate vaccination
894 after surgery for pet dogs with high-grade glioma. *Cancers (Basel)* 2019; **11**: 137.

895 65 Zhang S, Phillips JH. Identification of tyrosine residues crucial for CD200R-mediated
896 inhibition of mast cell activation. *J Leukoc Biol* 2005; **79**: 363–368.
897 66 Hatherley D, Lea SM, Johnson S, Barclay AN. Structures of CD200/CD200 receptor
898 family and implications for topology, regulation, and evolution. *Structure* 2013; **21**: 820–
899 832.
900 67 Luo ZX, Yuan CX, Meng QJ, Ji Q. A Jurassic eutherian mammal and divergence of
901 marsupials and placentals. *Nature* 2011; **476**: 442–445.
902 68 Wong KK, Khatri I, Shaha S, Spaner DE, Gorczynski RM. The role of CD200 in
903 immunity to B cell lymphoma. *J Leukoc Biol* 2010; **88**: 361–372.
904 69 Caserta S, Nausch N, Sawtell A, Drummond R, Barr T, MacDonald AS *et al.* Chronic
905 infection drives expression of the inhibitory receptor CD200R, and its ligand CD200, by
906 mouse and human CD4 T cells. *PLoS One* 2012; **7**: e35466.
907 70 Foster-Cuevas M, Westerholt T, Ahmed M, Brown MH, Barclay AN, Voigt S.
908 Cytomegalovirus e127 protein interacts with the inhibitory CD200 receptor. *J Virol* 2011;
909 **85**: 6055–9.
910 71 Foster-Cuevas M, Wright GJ, Puklavec MJ, Brown MH, Barclay AN. Human herpesvirus
911 8 K14 protein mimics CD200 in down-regulating macrophage activation through CD200
912 receptor. *J Virol* 2004; **78**: 7667–76.
913 72 Alves JM, Carneiro M, Cheng JY, Matos AL de, Rahman MM, Loog L *et al.* Parallel
914 adaptation of rabbit populations to myxoma virus. *Science* 2019; : eaau7285.
915 73 Barclay AN, Hatherley D. The Counterbalance Theory for Evolution and Function of
916 Paired Receptors. *Immunity* 2008; **29**: 675–678.
917 74 Tovar C, Obendorf D, Murchison EP, Papenfuss AT, Kreiss A, Woods GM. Tumor-

918 specific diagnostic marker for transmissible facial tumors of tasmanian devils:
919 Immunohistochemistry studies. *Vet Pathol* 2011; **48**: 1195–1203.
920 75 Marx V. Calling the next generation of affinity reagents. *Nat Methods* 2013; **10**: 829–833.
921 76 Grabherr MG, Haas BJ, Yassour M, Levin JZ, Thompson DA, Amit I *et al.* Full-length
922 transcriptome assembly from RNA-Seq data without a reference genome. *Nat Biotechnol*
923 2011; **29**: 644–52.
924 77 Kowarz E, Löscher D, Marschalek R. Optimized Sleeping Beauty transposons rapidly
925 generate stable transgenic cell lines. *Biotechnol J* 2015; **10**: 647–653.
926 78 Mátés L, Chuah MKL, Belay E, Jerchow B, Manoj N, Acosta-Sanchez A *et al.* Molecular
927 evolution of a novel hyperactive Sleeping Beauty transposase enables robust stable gene
928 transfer in vertebrates. *Nat Genet* 2009; **41**: 753–761.
929 79 Waldo GS, Standish BM, Berendzen J, Terwilliger TC. Rapid protein-folding assay using
930 green fluorescent protein. *Nat Biotechnol* 1999; **17**: 691–5.
931 80 Kozak M. An analysis of 5'-noncoding sequences from 699 vertebrate messenger RNAs.
932 *Nucleic Acids Res* 1987; **15(20)**: 8125–8148.
933 81 Gasteiger E, Hoogland C, Gattiker A, Duvaud S, Wilkins MR, Appel RD *et al.* Protein
934 identification and analysis tools in the ExPASy server. In: Walker JM (ed). *The*
935 *Proteomics Protocols Handbook*. Humana Press, 2005, pp 571–607.
936 82 Robinson M, McCarthy D, Smyth G. edgeR: a Bioconductor package for differential
937 expression analysis of digital gene expression data. *Bioinformatics* 2010; **26**: 139–140.
938
939
940

941

FIGURES

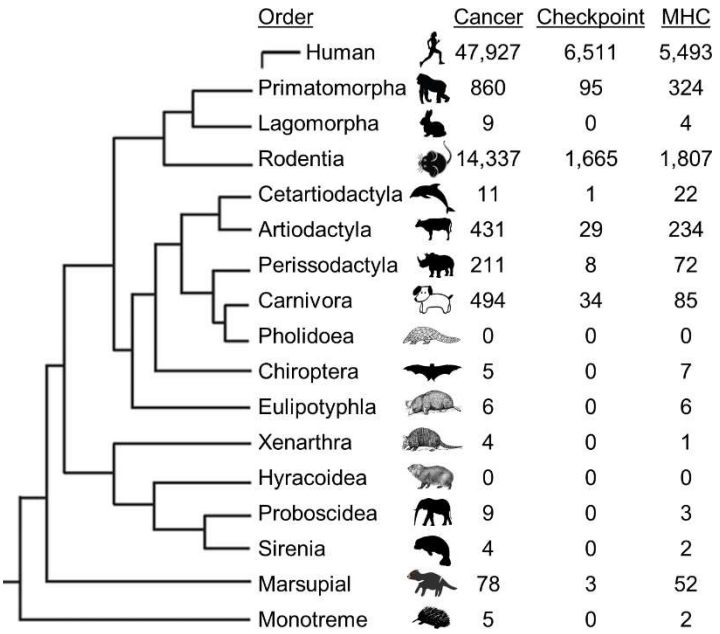

Figure 1. Phylogenetic tree of immune system related studies in mammal orders 2009-2019. Metastatic cancer has been reported in nearly all mammalian orders and major histocompatibility complexes (MHC) have been the most intensely studied molecules in most orders. In the past decade, studies of immune checkpoint molecules (PD1, PDL1, CTLA4) have become a primary focus in humans and rodents. However, immune checkpoint studies in other species are limited, particularly at the protein level, due to the lack of species-specific reagents. This creates a vast gap in our understanding of the evolution of the mammalian immune system. The numbers in the columns represent the number studies matching Web of Science search results between 2009-2019. See Table S1 for search terms.

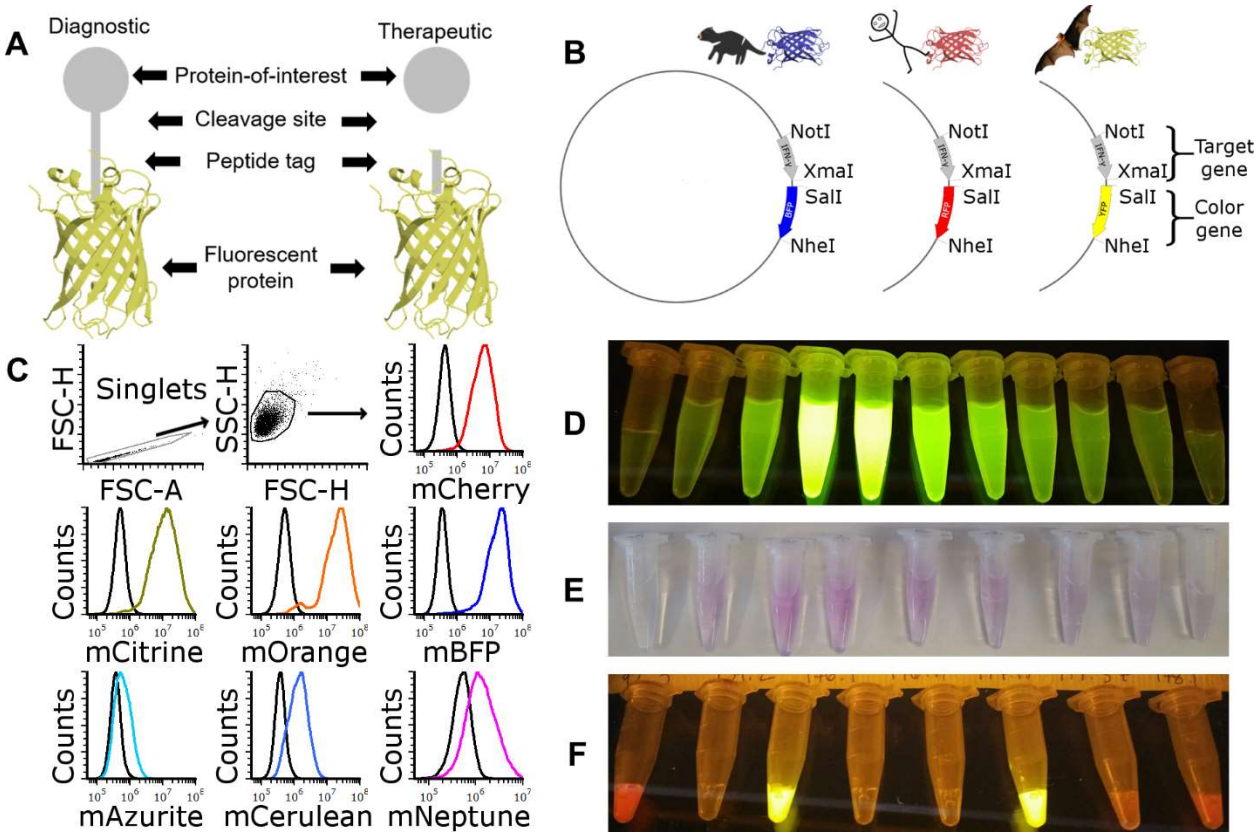

Figure 2. FAST protein schematic and initial testing. (A) Schematic diagram of FAST protein therapeutic and diagnostic (i.e. theranostic) features and (B) vector map showing restriction sites for swapping the target gene (i.e. gene-of-interest) and color genes (i.e. fluorescent protein). (C) Results of flow cytometry binding assay with devil 41BB FAST proteins. The colored lines in the histograms show binding of devil 41BB fused to mCherry, mCitrine, mOrange, mTagBFP, mAzurite, mCerulean3, or mNeptune2 to CHO cells transfected with devil 41BBL, and the black lines show binding to untransfected CHO cells. (D-E) Images showing the gradient of FAST proteins eluted from HisTrap columns. (D) mCitrine excited with blue light and (E) chromogenic visualization of mCherry without excitation. (F) Image of 100 µL of FAST protein excited with blue light (NOTE: mBFP appears clear with blue excitation and amber filter unit).

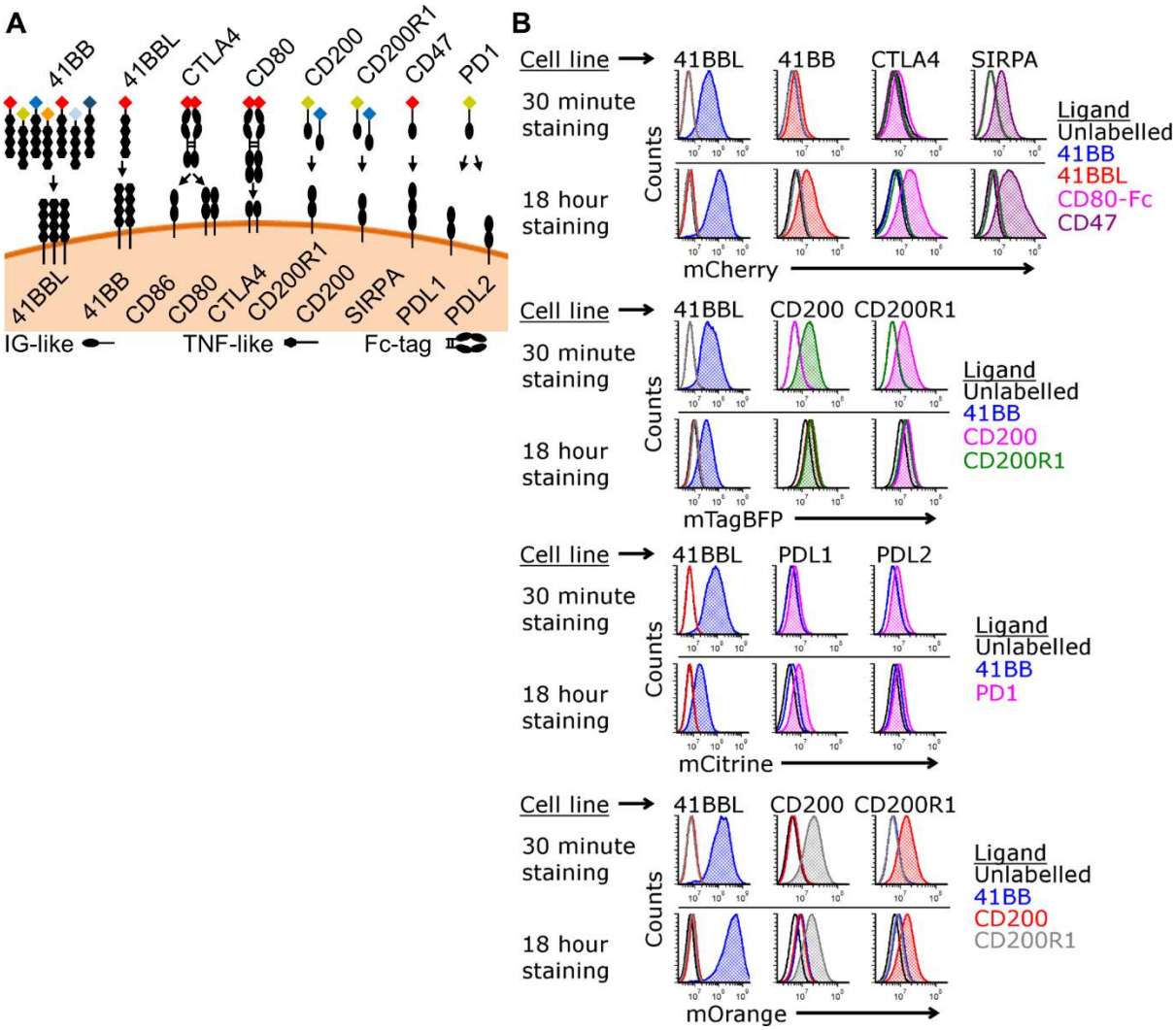

Figure 3. Map and testing of soluble proteins FAST proteins. (A) Diagram of soluble FAST proteins and full-length proteins used for testing of FAST proteins. 41BBL is a type II transmembrane protein; all other proteins are type I. CD80 and CTLA4 soluble FAST proteins included a devil IgG Fc-tag. Arrows indicate interactions confirmed in this study. (B) Histograms showing binding of FAST proteins to CHO cells expressing full-length devil proteins. Target CHO cells were cultured with chloroquine to block lysosomal degradation of FAST proteins and maintain fluorescent signal during live-culture binding assays with 2 µg/well of purified FAST proteins for 30 minutes or 18 hours to assess receptor-ligand binding (n=1/time point).

977

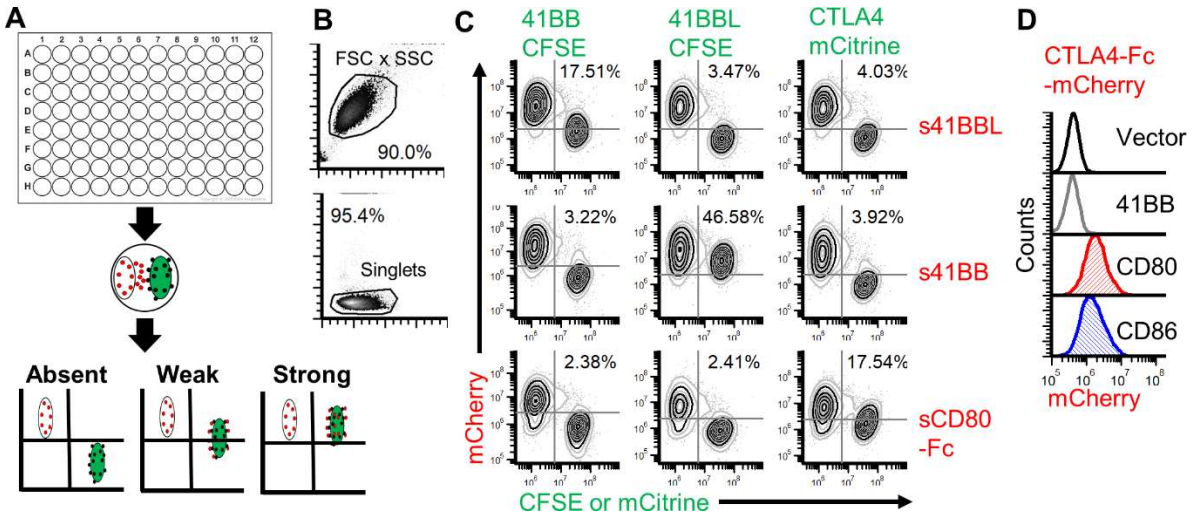

978 **Figure 4. Live-cell coculture assays with FAST proteins.** (A) Schematic of coculture assays to
979 assess checkpoint molecule interactions (Absent, Weak, Strong). Cells were mixed and cultured
980 overnight with chloroquine. Protein binding and/or transfer were assessed using flow cytometry.
981 (B) Gating strategy for coculture assays. (C) CHO cells that secrete 41BBL-mCherry, 41BB-
982 mCherry, or CD80-Fc-mCherry were cocultured overnight with target CHO cells that express full-
983 length 41BB, 41BBL, or CTLA4. 41BB and 41BB-L were labeled with CFSE, whereas full-length
984 CTLA4 was directly fused to mCitrine. Cells that secrete mCherry FAST proteins appear in the
985 upper left quadrant. Cells expressing full-length proteins and labeled with CFSE or mCitrine
986 appear in the lower right quadrant. Cells in the upper right quadrant represent binding of mCherry
987 FAST proteins to full-length proteins on CFSE or mCitrine labeled cells. Results shown are
988 representative of n=3/treatment. (D) CTLA4-Fc-mCherry FAST protein binding to DFT cells.
989 DFT1 C5065 cells transfected with control vector (black), 41BB (gray), CD80 (red), or CD86
990 (blue) were stained with CTLA4-Fc-mCherry supernatant with chloroquine. Results are
991 representative of n=2 replicates/treatment.

992

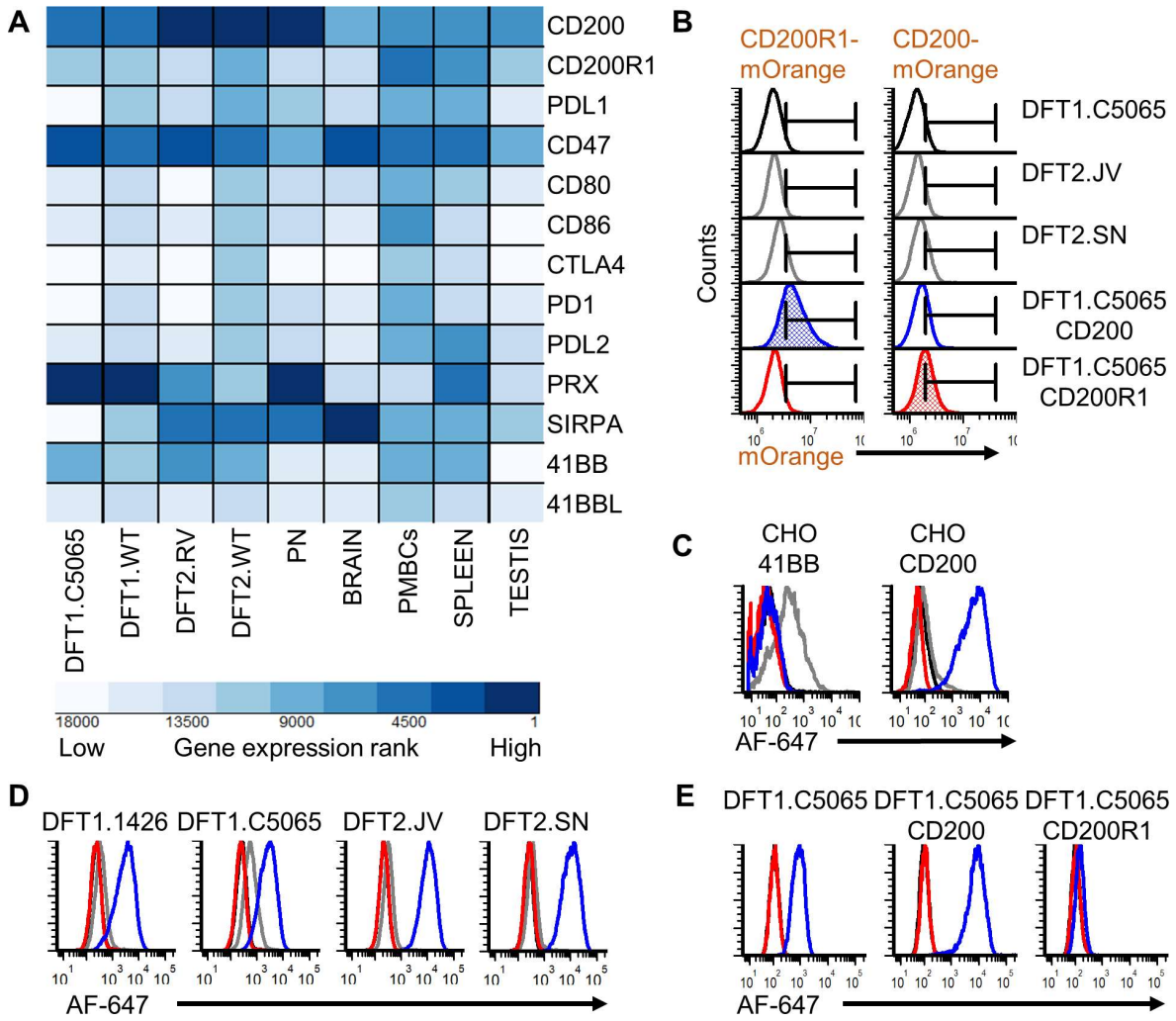

Figure 5. Elevated CD200 expression on DFT cells. (A) Heatmap showing within sample transcript ranking (1 = highest expression) according to RPKM-normalized mRNA sequencing counts of 18,788 annotated coding genes (devil_refv7.0; GCA_000189315.1). Genes-of-interest for this study are plotted as heatmap with dark blue indicating the most highly expressed genes. Technical replicates (n=2) were used for all tissues, except peripheral nerve (PN) (n=1). (B) Wild type DFT1.C5065, DFT2.JV, DFT2.SN, and DFT1.C5065 transfected to overexpress CD200 or CD200R1 were stained with 5 µg of either CD200R1-mOrange or CD200-mOrange FAST protein. Histograms filled with blue or red highlight the cells overexpressing CD200 or CD200R1 and their expected binding interactions with CD200R1 and CD200, respectively. Target cells were cultured

1003 with FAST proteins in chloroquine, incubated 30 minutes, and run without washing. Results are
1004 representative of n=2 replicates/treatment. (C) Mice were immunized with TEV digested 41BB or
1005 CD200 FAST proteins. Black = pre-immune (PI) and gray = immune (I) sera from a mouse
1006 immunized with 41BB; red = pre-immune (PI) and blue = immune (I) sera from a mouse
1007 immunized with CD200. CHO cells transfected with either full-length 41BB or CD200 were
1008 stained with sera and then anti-mouse AlexaFluor-647. Results are representative of
1009 n=2/treatment. (D) Sera was used to screen two strains of DFT1 and two strains of DFT2 cells for
1010 41BB and CD200 expression. PI sera was negative in all cases, whereas all DFT1 and DFT2 cells
1011 expressed CD200. Results are representative of n=3/treatment. (E) DFT1 C5065 transfected with
1012 either vector control, CD200, or CD200R1 were stained with purified polyclonal anti-CD200 and
1013 anti-mouse IgG AlexaFluor 647 (black = no antibodies, red = secondary antibody only, blue =
1014 primary + secondary antibody). Results are representative of n=2/treatment.
1015

1016

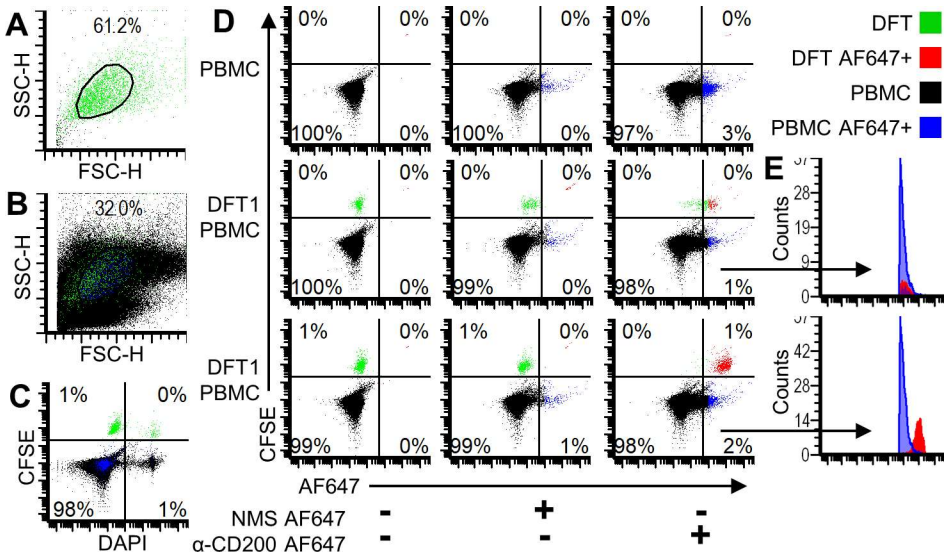

1017

1018 **Figure 6. CD200 identifies DFT cells in whole blood.** Color dot plots showing DFT cells in green
1019 (CFSE), PBMCs in black, DFT Alexa Fluor 647+ (AF647) cells in red, and PBMC AF647+ in
1020 blue. (A) Forward- and side-scatter plot of DFT.JV cells and (B) DFT.JV cells mixed with PBMCs.
1021 (C) Color dot plot showing dead cells stained with DAPI (right quadrants) and CFSE-labeled DFT
1022 cells (upper quadrants). (D) The top row shows unmixed PBMCs. The middle row and bottom row
1023 show DFT1.C5065 and DFT2.JV cells, respectively, mixed with PBMCs. Alexa Fluor 647+ DFT
1024 (red) and PBMC (blue) are in the right quadrants. (E) Histogram overlays to highlight AF647+
1025 (right quadrants) from DFT1-PBMC and DFT2-PBMC mixtures. Cells were analyzed on the
1026 Beckman-Coulter MoFlo Astrios.

1027

1028 **TABLES (See supplementary Materials)**

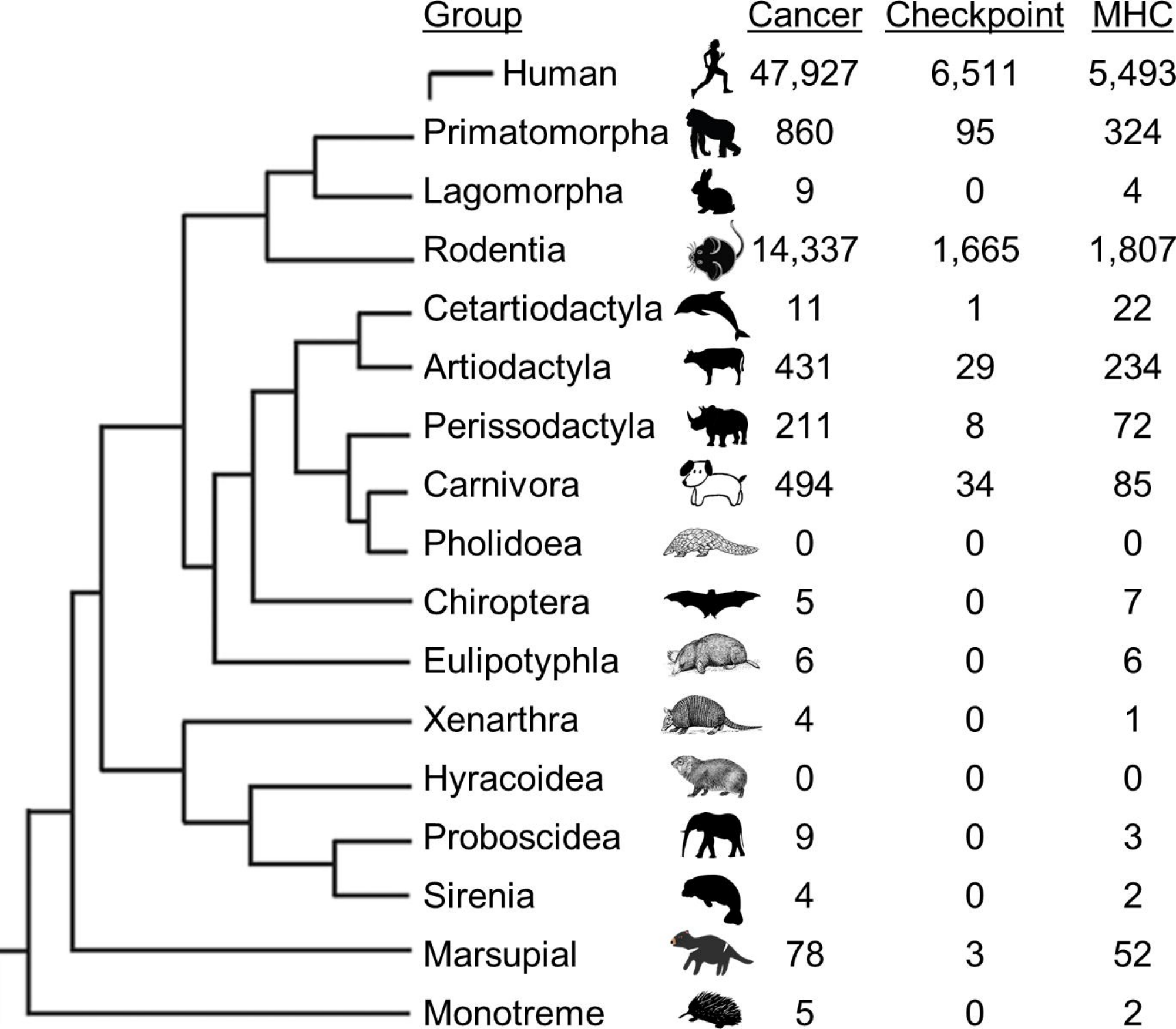
Group
Cancer
Checkpoint
MHC
Human 47,927 6,511 5,493
Primatomorpha 860 95 324
Lagomorpha 9 0 4
Rodentia 14,337 1,665 1,807
Cetartiodactyla 11 1 22
Artiodactyla 431 29 234
Perissodactyla 211 8 72
Carnivora 494 34 85
Pholidoea 0 0 0
Chiroptera 5 0 7
Eulipotyphla 6 0 6
Xenarthra 4 0 1
Hyracoidea 0 0 0
Proboscidea 9 0 3
Sirenia 4 0 2
Marsupial 78 3 52
Monotreme 5 0 2

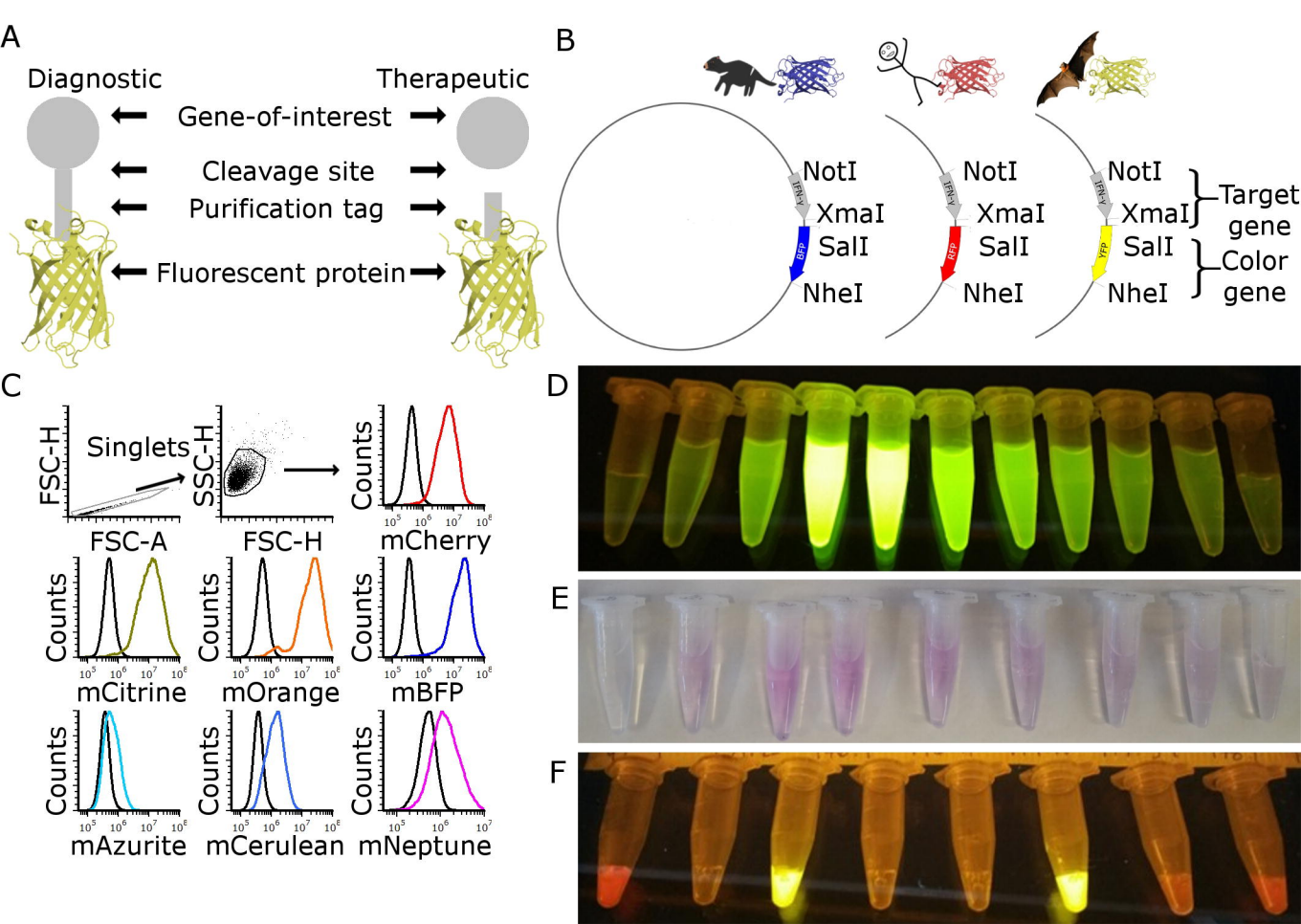
A
Diagnostic
Therapeutic
Gene-of-interest
Cleavage site
Purification tag
Fluorescent protein
B
NotI
XmaI
SalI
NheI
IFN-γ
BFP
RFP
YFP
Target gene
Color gene
C
Singlets
FSC-H
FSC-A
SSC-H
Counts
mCherry
mCitrine
mOrange
mBFP
mAzurite
mCerulean
mNeptune
D
E
F

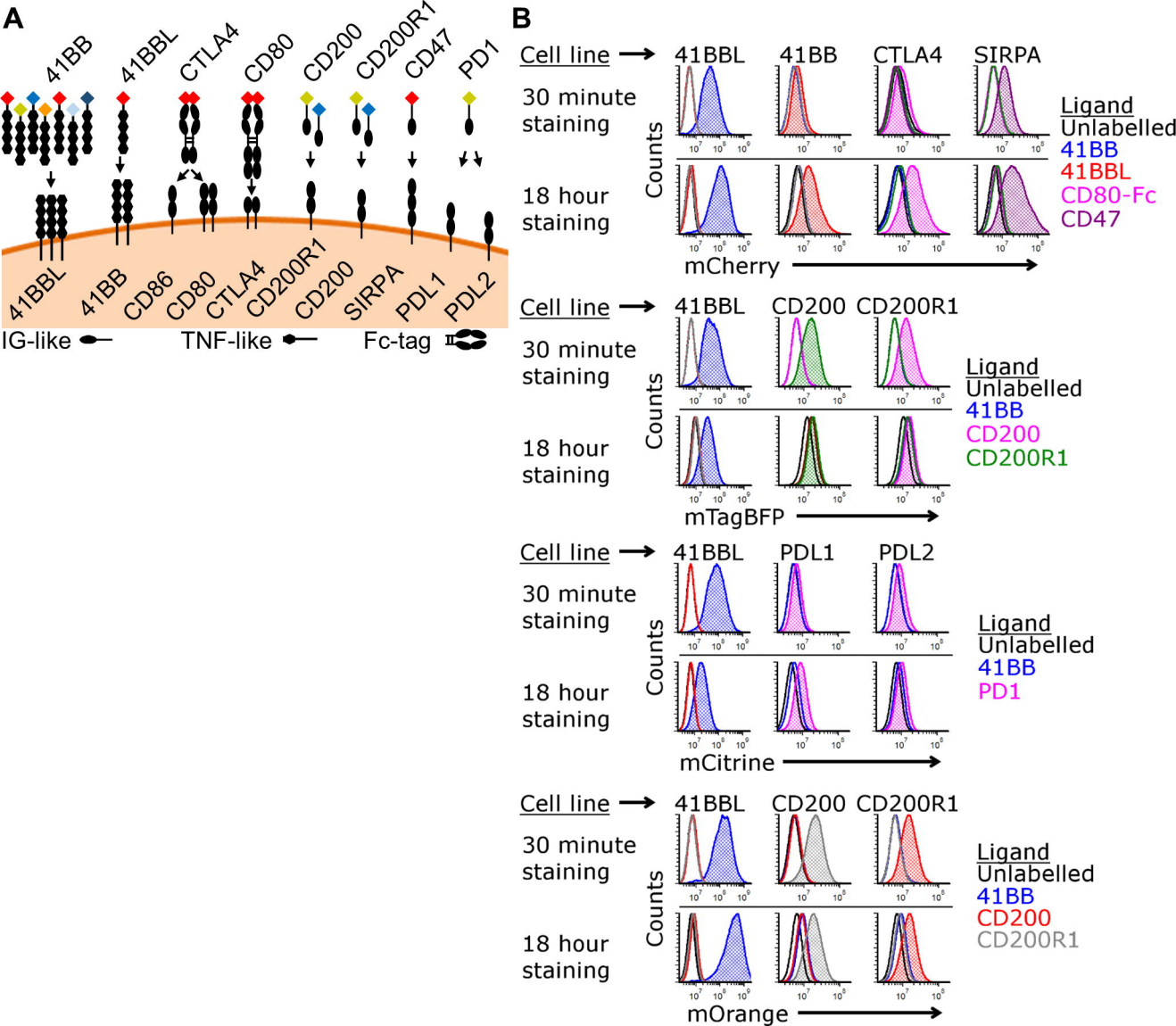
A
41BB
41BBL
CTLA4
CD80
CD200
CD200R1
CD47
PD1
41BBL
41BB
CD86
CD80
CTLA4
CD200R1
CD200
SIRPA
PDL1
PDL2
IG-like
TNF-like
Fc-tag
B
Cell line
41BBL
41BB
CTLA4
SIRPA
30 minute staining
18 hour staining
Counts
mCherry
Ligand
Unlabelled
41BB
41BBL
CD80-Fc
CD47
Cell line
41BBL
CD200
CD200R1
30 minute staining
18 hour staining
Counts
mTagBFP
Ligand
Unlabelled
41BB
CD200
CD200R1
Cell line
41BBL
PDL1
PDL2
30 minute staining
18 hour staining
Counts
mCitrine
Ligand
Unlabelled
41BB
PD1
Cell line
41BBL
CD200
CD200R1
30 minute staining
18 hour staining
Counts
mOrange
Ligand
Unlabelled
41BB
CD200
CD200R1

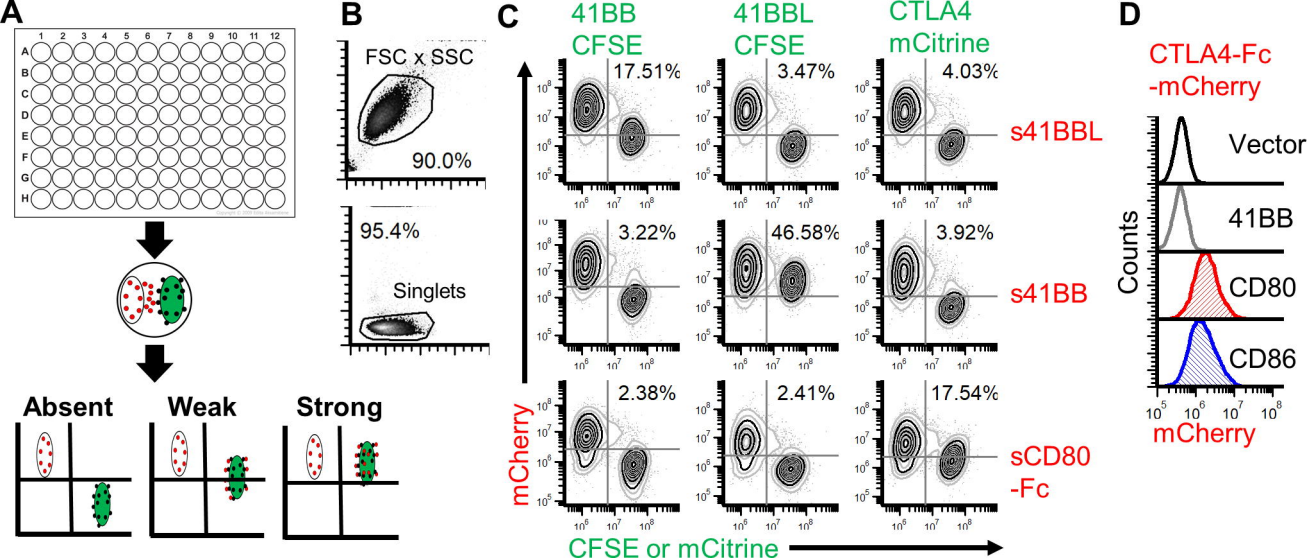
A
1 2 3 4 5 6 7 8 9 10 11 12
A B C D E F G H
Absent
Weak
Strong
B
FSC x SSC
90.0%
95.4%
Singlets
C
41BB CFSE
41BBL CFSE
CTLA4 mCitrine
17.51%
3.47%
4.03%
s41BBL
3.22%
46.58%
3.92%
s41BB
2.38%
2.41%
17.54%
sCD80 -Fc
mCherry
CFSE or mCitrine
D
CTLA4-Fc -mCherry
Vector
41BB
CD80
CD86
Counts
mCherry

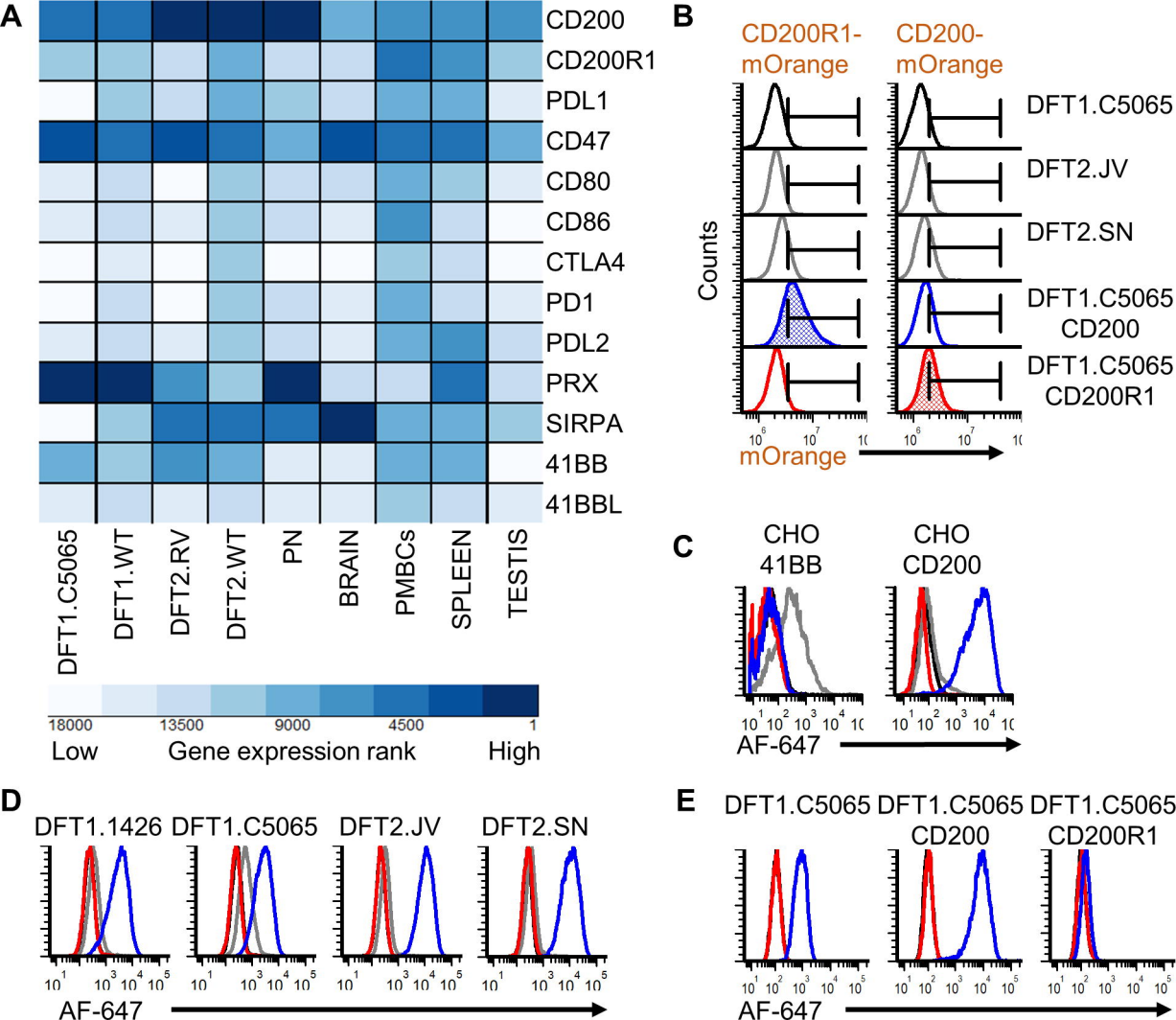
A
CD200
CD200R1
PDL1
CD47
CD80
CD86
CTLA4
PD1
PDL2
PRX
SIRPA
41BB
41BBL
DFT1.C5065
DFT1.WT
DFT2.RV
DFT2.WT
PN
BRAIN
PMBCs
SPLEEN
TESTIS
18000
13500
9000
4500
1
Low
Gene expression rank
High
B
CD200R1-mOrange
CD200-mOrange
DFT1.C5065
DFT2.JV
DFT2.SN
DFT1.C5065 CD200
DFT1.C5065 CD200R1
Counts
mOrange
C
CHO 41BB
CHO CD200
AF-647
D
DFT1.1426
DFT1.C5065
DFT2.JV
DFT2.SN
AF-647
E
DFT1.C5065
DFT1.C5065 CD200
DFT1.C5065 CD200R1
AF-647

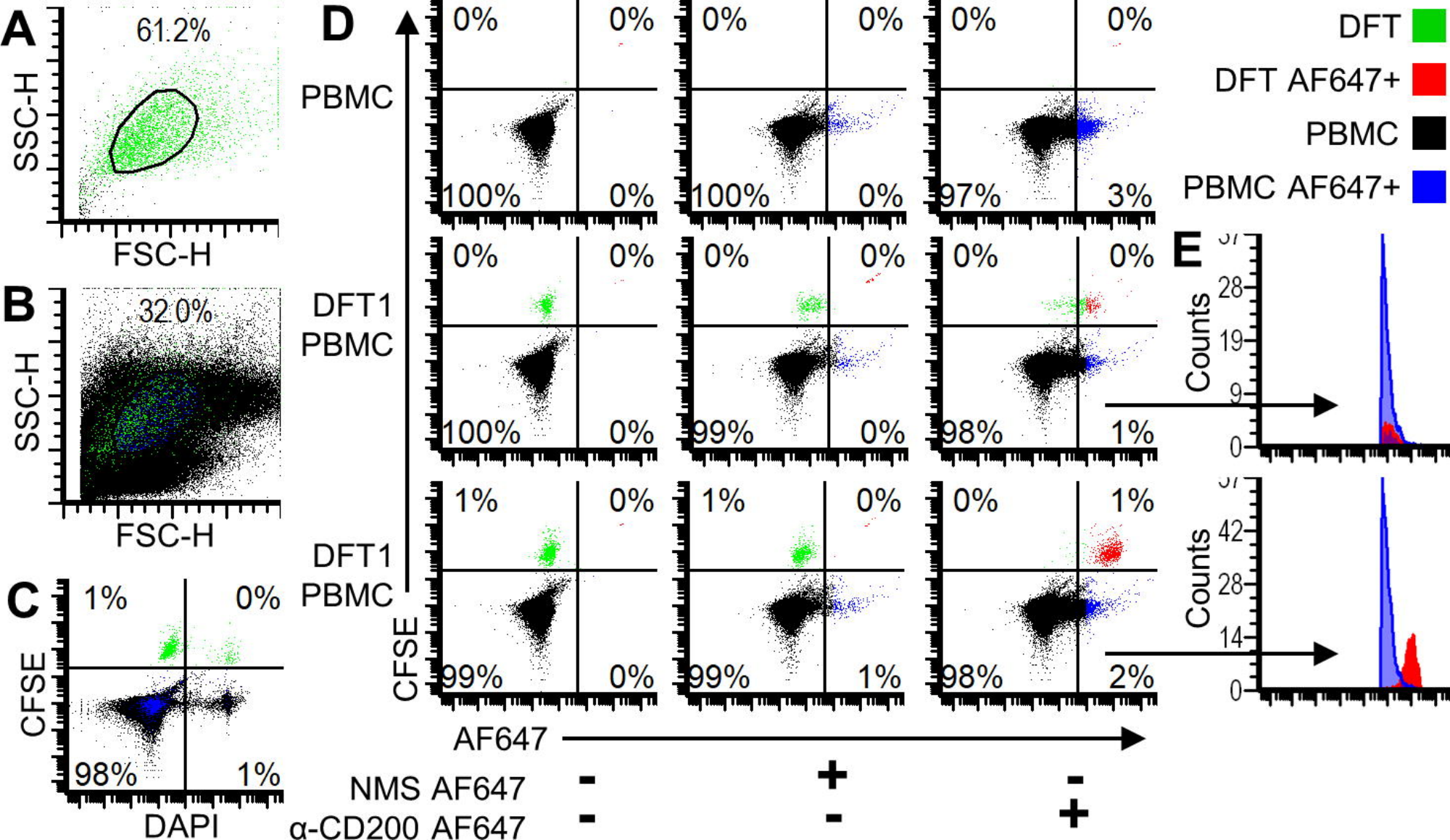
A
61.2%
SSC-H
FSC-H
B
32.0%
SSC-H
FSC-H
C
1%
0%
CFSE
98%
1%
DAPI
D
PBMC
DFT1
PBMC
DFT1
PBMC
0%
0%
100%
0%
0%
0%
100%
0%
0%
0%
97%
3%
0%
0%
100%
0%
0%
0%
99%
0%
0%
0%
98%
1%
1%
0%
99%
0%
1%
0%
99%
1%
0%
1%
98%
2%
CFSE
AF647
NMS AF647
α-CD200 AF647
DFT
DFT AF647+
PBMC
PBMC AF647+
E
Counts
28
19
9
0
Counts
42
28
14
0